SCOUR AT REAR SIDE OF A COASTAL REVETMENT DUE TO SOLITARY-LIKE WAVE OVERTOPPING

A THESIS SUBMITTED TO
THE GRADUATE SCHOOL OF NATURAL AND APPLIED SCIENCES
OF
MIDDLE EAST TECHNICAL UNIVERSITY

BY

MERT YAMAN

IN PARTIAL FULFILLMENT OF THE REQUIREMENTS
FOR
THE DEGREE OF MASTER OF SCIENCE
IN
CIVIL ENGINEERING

MAY 2022

Approval of the thesis:

SCOUR AT REAR SIDE OF A COASTAL REVETMENT DUE TO SOLITARY-LIKE WAVE OVERTOPPING

submitted by **MERT YAMAN** in partial fulfillment of the requirements for the degree of **Master of Science** i**n Civil Engineering, Middle East Technical University** by,

Prof. Dr. Halil Kalıpçılar
Dean, Graduate School of **Natural and Applied Sciences** _____

Prof. Dr. Erdem Canbay
Head of the Department, **Civil Engineering** _____

Prof. Dr. Ahmet Cevdet Yalçıner
Supervisor, **Civil Engineering, METU** _____

Assist. Prof. Dr. Cüneyt Baykal
Co-Supervisor, **Civil Engineering, METU** _____

Examining Committee Members:

Assist. Prof. Dr. Gülizar Özyurt Tarakcıoğlu
Civil Engineering, METU _____

Prof. Dr. Ahmet Cevdet Yalçıner
Civil Engineering, METU _____

Assist. Prof. Dr. Cüneyt Baykal
Civil Engineering, METU _____

Assoc. Prof. Dr. Mustafa Tuğrul Yılmaz
Civil Engineering, METU _____

Assist. Prof. Dr. Doğan Kısacık
Civil Engineering, IZTECH _____

Date: 11.05.2022

I hereby declare that all information in this document has been obtained and presented in accordance with academic rules and ethical conduct. I also declare that, as required by these rules and conduct, I have fully cited and referenced all material and results that are not original to this work.

Name Last name : Mert Yaman

Signature :

ABSTRACT

SCOUR AT THE REAR SIDE OF RUBBLE MOUND REVETMENT DUE TO THE SOLITARY-LIKE WAVE OVERTOPPING

Yaman, Mert
Master of Science, Civil Engineering
Supervisor : Prof. Dr. Ahmet Cevdet Yalçıner
Co-Supervisor: Assist. Prof. Dr. Cüneyt Baykal

May 2022, 58 pages

Rubble mount coastal structures are commonly used for protecting coastal utilities. Under storm conditions or extreme conditions, long waves attack those structures and cause overtopping. This overtopping phenomenon often results in water flow at the back side of the structure which consequently causes scour. In this thesis, different solitary-like waves and the backfill conditions are studied to understand the level of overtopping and maximum scour depth behind the structure due to the solitary-like wave caused by overtopping. The relation between the scour and sediment characteristics, wave, and overtopping conditions are investigated and dimensionless figures are developed for the generalization of the results in the range of physical experiments. The main finding of this study is that average overtopping discharge is directly related to the maximum scour behind the revetment structure. Another finding is that grain size diameter of the backfill material and backfill height are governing parameters of scour. Moreover, it is investigated that number of overtopped solitary-like waves causes a gradual increase in scour depth for the first few attacks of solitary waves, and then the increment becomes less for the rest of the wave attacks.

Keywords: Solitary Wave, Coastal Revetment, Scour

ÖZ

KIYI KORUMA YAPILARI ARKASINDA SOLİTER BENZERİ DALGALARIN AŞMASI NEDENİYLE OLUŞAN OYULMA

Yaman, Mert
Yüksek Lisans, İnşaat Mühendisliği
Tez Yöneticisi: Prof. Dr. Ahmet Cevdet Yalçıner
Ortak Tez Yöneticisi: Dr. Öğr. Üyesi Cüneyt Baykal

Mayıs 2022, 58 sayfa

Taş dolgu kıyı yapıları kıyı koruma amaçlı olarak sıklıkla kullanılmaktadır. Fırtına ya da ekstrem durumlarda uzun dalgalar bu yapıları etkiler ve dalga aşımına neden olur. Bu dalga aşımı, kıyı yapısının arkasında su akışına neden olur ve oyulma gözlemlenir. Bu tezde, dalga aşım seviyesini ve neden olduğu en yüksek oyulma değerini anlamak için birbirinden farklı soliter benzeri dalgalar ve farklı özellikteki arka alan dolguları çalışılmıştır. Sonuçların genellenmesi için oyulma ve sediman karakteristiği, dalga ve aşım durumları araştırılmış, boyutsuz figürler geliştirilmiştir. Çalışmanın ana bulgularından biri ortalama aşma debisinin maksimum oyulma derinliğiyle doğrudan ilişkili olduğunun bulunmasıdır. Bir başka bulgu ise arka alan sediman dane çapının ve arka alan derinliğinin oyulma üzerinde etkili parametreler olduğunun anlaşılmasıdır. Ayrıca, aşan soliter benzeri dalgaların oyulma çukurunu kademeli şekilde artırdığıdır.

Anahtar Kelimeler: Soliter Dalga, Kıyı Tahkimatı, Kıyı Koruma Yapısı, Oyulma

Dedicated to my father

ACKNOWLEDGMENTS

First, I would like to express my deepest gratitude to my advisors Prof. Dr. Ahmet Cevdet Yalçıner and Assist. Prof. Dr. Cüneyt Baykal. This study would not be possible to be completed without their help. Prof. Dr. Ahmet Cevdet Yalçıner has always supported me during the experimental stage and after the experiments were finished. His support made me keep working on this study. Assist. Prof. Dr. Cüneyt Baykal was always on the other side of his phone regardless of the time. During the long night shifts of our physical experimental stage, he helped us from afar. Without him, analysis of the valuable physical experimental results would not be possible. His help in this study can not be expressed in words.

I would like to extend my sincere thanks to Prof. Dr. Ayşen Ergin who convinced me to be a coastal engineer even in her first hour of the class CE491. Her positive attitude did not only guide my research but also guided my understanding of life. I am very lucky to be one of her students in her magnificent academic life.

Dr. Işıkhan Güler is one of the hidden leading actors in this study to be completed. His support both in university and in life can not be expressed in words. I am lucky to be one of his students and his colleague. There is a lot more to learn from him in the future.

I would like to express my gratitude to Assist. Prof. Dr. Gülizar Özyurt Tarakcıoğlu. The course CE496 made up my mind and supported my will to be a coastal engineer.

I would like to express my gratitude to Dr. Hasan Gökhan Güler and Gözde Güney Doğan Bingöl. Dr. Hasan Gökhan Güler is always there for all of the students not only for academic purposes. He always supported me in this study and with our discussions on life, technology, and engineering, he had a big role in how an engineer I am today. Gözde Güney Doğan Bingöl is both an instructor and a friend for me. Her support can not be limited to academic life but to everything that I encountered during our time in this laboratory. I am lucky to have a friend like her.

I would like to express my appreciation to my laboratory brother Mehmet Emre Yıldırım for his continuous will to complete the tasks we encountered. We have conducted experiments for almost a year without almost any breaks. He made us keep going when we were in our worst conditions and his commitment was priceless.

I would like to thank our laboratory technician Yusuf Korkut for his help during the physical experiments. We had long shifts without any problem.

I would like to especially thank my friends Barış Ufuk Şentürk, Cem Sevindik, Furkan Demir, and Berkay Erler, for their support in the last stage of the writing stage of this thesis. They have shared the late nights with me to correct and shape this thesis.

I would like to thank my friends Kadir Karakaş, İlker Çoban, Cem Bingöl, Koray Deniz Göral, Can Özsoy, Sedat Gözlet, Ghazal Khodkar, Utku Uzun, Aslıhan Devran, Arda Çiçek, Berkay Akyol, Bilge Karakütük and Günay Gazaloğlu who I met and worked together in my time in this laboratory.

I would like to thank my family for their support during my graduate study. I wish my father could see the completion of this thesis. May he rest in peace.

Lastly, I would like to express my gratitude to Dolfen Engineering Consultancy for supporting me to finish this study by providing me with a flexible work environment.

This work is partly funded by the Scientific and Technological Research Council of Turkey under grant number TUBİTAK 119M677.

TABLE OF CONTENTS

LIST OF TABLES

TABLES

LIST OF FIGURES

FIGURES

LIST OF ABBREVIATIONS

ABBREVIATIONS

CFD	Computational Fluid Dynamics
COBRAS	Concrete Bridge Assessment Program
DHI	Danish Hydraulic Institute
KC	Keulegan-Carpenter Number
METU	Middle East Technical University

LIST OF SYMBOLS

SYMBOLS

A	Maximum Accretion Height at the Rear Side of the Revetment
c	Wave Celerity
d_{16}	Median Diameter of Sediment Finer than 16%
d_{50}	Median Diameter of Sediment Finer than 50%
d_{84}	Median Diameter of Sediment Finer than 84%
Δ	The Ratio of Submerged Backfill Material Weight and Water Weight
η	Water Surface Elevation
Fr	Froude Number
Fr_m	Froude Number of Model
Fr_p	Froude Number of Prototype
g	Gravitational Acceleration
G_c	Crest Width
h_0	Water Jet Thickness
h_c	Backfill Height
h_{toe}	Water Depth at the Toe of The Revetment
H_{toe}	Solitary Wave Height at the Toe of the Revetment
k_{decay}	Outskirt Decay Coefficient
ξ	Trajectory of Paddle
L_A	Width of Accretion in Wave Direction

λ_L	Length Scale
λ_Q	Scale of Overtopping
λ_t	Time Scale
λ_W	Weight Scale
L_{rep}	Representative Solitary Wave Length
L_s	Width of Scour Hole in Wave Direction
m	Bed Slope
n	Porosity
N	Number of Solitary Wave Attack
q_{avg}	Average Overtopping Discharge Per Unit Width
R_c	Crest Height
ρ_s	Density of Sediment
ρ_w	Density of Water
S	Maximum Scour Depth at the Rear Side of the Revetment
σ	Grain Size Distribution
t	Time
tan_α	The slope of the Revetment
τ	Bed Shear Stress on the Backfill Surface
τ_{cr}	Critical Shear Stress of the Backfill Material
V	Water Jet Velocity
w_s	Fall Velocity of Sediment
x	Coordinate in the Wave Approach Direction

x_A	Distance of Maximum Accretion Height from the Crown Wall
x_S	Distance of Maximum Scour Depth from the Crown Wall
z	Coordinate Perpendicular to the Wave Approach Direction

CHAPTER 1

INTRODUCTION

Coastal revetments are built to protect coastal areas and communities all around the world. These structures experience different water levels, wave conditions, and extreme events like severe storms or even tsunamis throughout their economic life. Revetment designs consider backfill area protection as well as they consider structural integrity. One of the phenomena that directly affect the backfill area is wave overtopping. Wave overtopping can be simply explained as the passing of water over the structure.

Wave overtopping causes local erosion, which is called scour, at the rear side of the revetment structure. Scour may show different effects at the rear side depending on the usage of the area. It can affect the stability of the revetment itself or it may cause damage to the roads, buildings, and people located at the rear side.

One of the commonly used revetment types is rubble mound revetments, which generally contain an armour layer of bigger rocks (boulders), a filter layer of smaller rocks, and a core layer of finer rocks. Rubble mound revetments are used in Türkiye coasts especially in Karadeniz and Akdeniz regions in order to protect the coastal zones.

In this study, morphological changes at the rear side of a rubble mound revetment due to solitary wave overtopping are investigated via physical model experiments. The scouring process is considered to occur in the conditions of either the structural process is not completed, or the rear side is filled with non-cohesive materials. The following questions are targeted to be answered by the scope of this study:

i. How do different wave conditions affect the scouring process under the same structural and morphological conditions?

ii. How is the scour depth at the rear side of rubble mound revetment related to the overflow jet thickness, velocity and duration, number of waves, grain size of backfill material and backfill height?

In Chapter 2, the literature surveyed is presented briefly. In Chapter 3, the methodology of this thesis is explained in different sub-sections, in detail. The results and findings of the physical model experiments and data analysis are presented in Chapter 4. The discussions on the results and conclusion of this thesis are presented in Chapter 5.

CHAPTER 2

LITERATURE REVIEW

This study investigates morphological changes at the rear side of a coastal revetment due to tsunami overflow thus, literature research has been done in the scope of the study. Research in literature related to the tsunami waves, overflow, tsunami induced scour, tsunami and structure interaction, also, solitary wave models and experiments are reviewed and a short brief is presented.

2.1 Tsunami Induced Scour Studies

Kato et al. (2001) investigated the effects of grain size on scouring around a cylinder due to tsunami runup. Conducted experiments with sand and gravel beds for cylindrical structure and gathered flow velocity, water depth, and pore pressure during the scour process. They concluded that the replacement of sand with gravel had reduced the scour area but it had not always affected the maximum scour depth. Kobayashi and Lawrence (2004) investigated cross-shore sediment transport under solitary wave breaking. They performed a series of tests containing positive and negative solitary waves and compared the runups and sediment suspension volumes. They concluded that a single solitary wave is capable of noticeable beach profile change. . Chiew, Lim, and Cheng (2004) investigated the mechanism of scour due to tsunami runup. The authors investigate a series of tsunami model experiments on a coastal cylindrical structure. They observed the most severe scour effect at the end of the drawdown phase of the tsunami and explained this behavior by pore-pressure gradients. Nakamura, Kuramitsu, and Mizutani (2008) conducted experiments and numerical simulations to understand tsunami-induced local scour around a structure, which had a square cross-section and on a sand foundation. They observed that at the seaward corner of the structure, relative overtopping height had a significant

effect on the scour depth as maximum scour was observed at the same location. Tsujimoto et al., (2008) investigated spectral evolution and time-space variations of sand beaches under tsunami waves and regular wave attacks. They performed experiments by generating negative and positive solitary waves, subjecting the beach to these generated waves, and gathered information on the recovery process by regular waves after tsunami events. . Larsen et al. (2018) focus on scour around monopile foundations due to tsunamis by applying a time-varying current. They investigate the final scour profile and summarize the prediction of the scour development is compatible with the fully coupled hydrodynamic and morphologic CFD model. Regarding the scour studies around pile breakwaters, Xu, Huang, and Yao (2019) investigated the effects of solitary wave parameters on maximum scour, accretion depth, and volumes of sedimentation as they conclude maximum scour depth and total scour volume are reliable parameters under highly nonlinear wave conditions regarding the validation of numerical models.

2.2 Tsunami and Structure Interaction Studies

Huang and Dong (2001) numerically investigated solitary wave and coastal dike interaction. They found out that two vortex generations at the lee side and at the toe of the dike, respectively, may cause scour and affect the stability of the dike. Liu and Tao (2004) studied the interaction of solitary waves with semi-circular breakwaters by numerical models and verified the model with experimental data. They investigated the vortex generation in different situations where breakwater is submerged, at the same level as the water level, and emerged. They conclude their findings may be used to understand contamination transport and transportation of suspended sediment Young and Testik (2009) conducted experiments with normally incident monochromatic waves applied to submerged vertical and semicircular breakwaters to understand the scour mechanism because of tsunami wave breaking. They concluded the scour mechanism is independent of breakwater type but depends on the KC number and they divided scour mechanism into two regimes that rely on

the KC number. Xiao, Young, and Prévost (2010) studied hydrodynamic and morphodynamic modeling of breaking solitary waves. They conducted their experiments over a fine sand beach. They focused on understanding the erosion mechanism due to the tsunami by observing the effect of the breaking solitary waves and also, providing the experimental data for validation of further numerical studies to predict erosion and deposition processes after a tsunami event. They concluded that the most significant sediment transport occurred during the drawdown phase and they observed net erosion on shore and the beach. Hsiao and Lin (2010) investigated tsunami-like solitary waves that overtop a seawall. They have conducted experiments and studied the numerical model COBRAS which is based on Reynolds-averaged Navier-Stokes equations. Their experiments contained three different cases, and they gave special attention to the vortex evolutionary behavior behind the sea wall. Chen et al. (2013) investigated tsunami-induced scour on coastal roadways. Their focus in the study is understanding the potential tsunami damage on roadways and enabling a path to plan disaster relief more efficiently. The authors conclude one of the most important factors to limit the scour is the distance between roadway and shoreline by presenting laboratory experiment results. Chen et al. (2016) expanded the discussion by studying tsunami-induced scour with protection by offshore breakwaters. They define important parameters to create empirical relations to understand local scour around the breakwater and assess potential tsunami damage to prevent excessive damage. They also mention that the submerged breakwaters are not effectively reducing the tsunami-induced scour but affect the erosion and deposition of sediment bars. Tsai et al. (2016) investigated the effects of the breakwater on solitary waves by numerical simulations based on Reynolds-averaged Navier-Stokes equations. They found the results of a significant reduction of the runup heights with increasing breakwater heights. On the other hand, the height increase of the breakwater resulted in increased forces on the structure at the top part. Jiang et al. (2017) investigated the interaction of tsunami-like solitary waves and seawalls. They have conducted their numerical simulations on OpenFOAM® using Navier-Stokes equations and by subjecting a rectangular seawall to solitary waves,

they analyzed wave and flow fields, overtopping discharge, and wave force. McGovern et al. (2019) focused on scour at onshore structures through experimental observations. They generated long waves in the laboratory environment to simulate tsunami scenarios with different inundation durations and they conclude that the increase in inundation duration increases scour depth as well. Mcgovern, Rossetto, and Todd (2019) continued their investigations on tsunami scour and they included tsunami wave forces at onshore structures. They performed experiments with different structural features and concluded that hydrostatic loading is higher than hydrodynamic loads in tsunami events.

Even though the literature mentioned above is related to this study, the main scope is to estimate scour at the rear side of a coastal protection structure (rubble mound revetment in this thesis) and the literature below is directly related to the focus of the experiments that shape this study.

Kato et al. (2012) studied the coastal dike failures due to the 2011 Great East Japan tsunami. They investigated failure patterns and concluded that scour at the landward toe of the dikes is the dominant failure pattern. Bricker, Francis, and Nakayama (2012) investigated scour depths around coastal structures after the 2011 tsunami. They compared measurements of the after-disaster surveys with theoretical and empirical methods. Authors studied the scour depths, caused by the overtopping of the tsunami on floodwalls and local scour around building foundations. Tanaka and Sato (2015) investigated the scoured regions behind embankments generated after the 2011 Great East Japan tsunami. They conducted their research that focuses on estimating the damage and hydraulic features of the tsunami. They observed that overflow type affects the scour characteristics greatly and the maximum energy head is related to the maximum scour depth. Nakamura et al. (2015) carried out a numerical model study to investigate local scour at the landward toe of a coastal dike due to tsunami overflow. They verified their numerical study outputs with physical experiment data and investigated tsunami force on armor blocks of the dike. They concluded that armor blocks at the landward side of the dike are vulnerable to the tsunami overflow because of the pore pressure increase and decrease in the water

pressure. (Wang et al. 2015a) studied scour behind seawalls due to the tsunami overflow by conducting numerical simulations. They summarized that the maximum scour depth behind the seawall is proportional to the overflow height. They also mentioned that the falling height of the overflow is inversely proportional to the scour depth.

Scour mechanism behind seawalls from tsunami overflow is studied by Wang et al. (2015b) as well. They carried out experimental and numerical studies to understand the mechanism and studied an optimum condition to reduce tsunami wave energy behind the seawall with an artificial trench. They concluded that the scour behind the seawall is rapidly generated with the start of the overflow. They also observed that an artificial trench is an effective solution to reduce the tsunami wave energy behind the seawall. Jayaratne et al. (2016), identified the failure mechanisms of coastal protection structure after the 2011 tsunami by investigations of post-tsunami surveys carried out between 2011 and 2013. They categorized the failure mechanisms, one of them being local scour at the landward toe of the dikes, and proposed a mathematical model to predict scour depth at the leeward toe of the coastal dikes considering soil properties, tsunami hydrodynamics, and structure type. Okura and Hiraishi (2018) studied scour behind seawalls due to overflowing tsunamis. They conduct physical experiments with solitary and long sinusoidal waves and investigated the sand ground behind the seawall after the tsunami attacked the seawall. They conclude that wave pressure of the ground behind the seawall may become large during a big tsunami event and appropriate measures must be taken into consideration in the design process. Rahman, Tanaka, and Reheman (2021) carried out experiments to reduce the scour and tsunami energy at the rear side of a seaward embankment with a double layer of vegetation. They used gravel as bed material and their analysis results showed that the double vegetation is a significantly efficient way to reduce scouring and tsunami energy.

CHAPTER 3

METHODOLOGY

A series of physical model experiments are conducted to investigate changes at the rear side of the revetment due to the overtopping of the solitary-like waves. The methodology for this investigation consists of six stages. In the first stage, a dimensional analysis using all involved parameters is conducted to evaluate the importance of the parameters before the experiments started. In the second stage, the scaling of the model is determined to construct the revetment model. Later, the experimental setup is built as the necessary parameters are determined. Afterward, solitary-like waves are generated and calibrated in the wave flume. In the sixth stage, the overtopping of solitary-like waves is measured, and scour measurements are conducted. In the upcoming sub-sections, these stages are explained respectively.

3.1 Dimensional Analysis

The structure used in the experiments is a rubble mound revetment which has a core, a filter, and an armour layer. In addition, a crown wall was placed from the top of the crest to the core layer, at the back side of the structure.

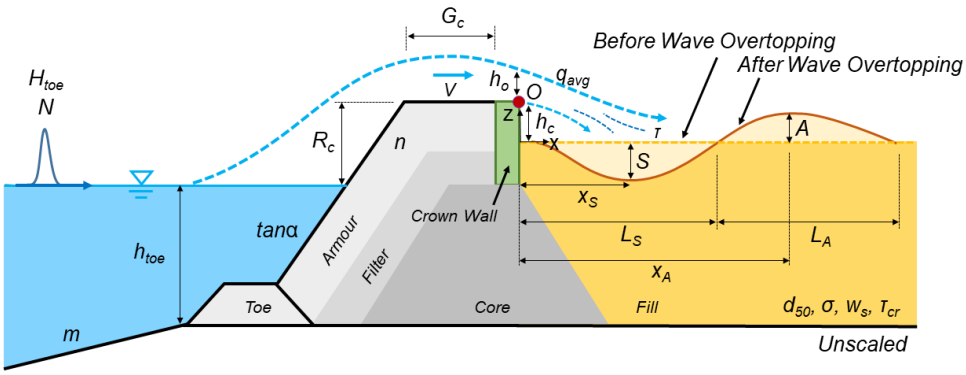

Figure 3.1 Parameters regarding the experimental setup (Adopted from Yildirim 2021))

The parameters are shown in Figure 3.1 related to the revetment structure, overtopping, scour, and accretion process behind the revetment. R_c crest height (m), G_c crest width (m), tan α front slope of the structure $(1V: 1.5H)$, n porosity and h_c backfill height (m) and h_{toe} water depth at the toe of the revetment $(0.27\ m)$ are structure related parameters. Parameters related to overflow are, H_{toe} solitary wave height (m) at the toe of the revetment, L_{rep} representative solitary wave length (m), N number of solitary wave attack the structure during the experiment session, h_0 water jet thickness (m), V water jet velocity (m/sn), ρ_w the density of water (kg/m^3), q_{avg} average overtopping discharge per unit width $(m^3/s/m)$. Parameters related to backfill material are, d_{16}, d_{50} and d_{84} the median diameter of the backfill material (m) that sediments are finer than $16\%, 50\%$ and 84% in volume, respectively, σ grain size distribution of the sediment d_{84}/d_{16}, ρ_s the density of the sediment (kg/m^3), τ bed shear stress on the backfill surface (Pa), τ_{cr} critical shear stress of the backfill material (Pa), w_s fall velocity of sediment (m/s). Rest of the parameters are, g gravitational acceleration $(9.81\ m/s^2)$, S maximum scour depth (m) at the rear side of the revetment, x_S distance of maximum scour depth from the crown wall (m), L_S width of scour hole in wave direction (m), A maximum accretion height (m), x_A distance of maximum accretion height from the crown wall (m), L_A width of accretion in wave direction (m), m the bed slope $(1: 20)$, x coordinate in the wave approach direction (m), z coordinate perpendicular to the wave approach direction (m) and t time (s).

Investigation of morphological changes at the rear side of the rubble mound revetment due to solitary wave overtopping may be expressed as Equation (3.1), related to the parameters mentioned above.

$$\varphi\begin{pmatrix} H, & L_{Rep}, & N, & tan\alpha, & m, & h_{toe}, & n, & R_c, & G_c, & h_c, \\ h_0, & d_{50}, & \sigma, & g, & \rho_s, & \rho_w, & q_{avg}, & V, & \tau, & \tau_{cr}, \\ w_s, & S, & A, & x_S, & x_A, & L_S, & L_A, & x, & z, & t \end{pmatrix} = 0 \qquad (3.1)$$

Parameters V and τ could not be measured during the experiments and they are

excluded from Equation (3.1). In addition, τ_{cr} and w_s are directly dependent on d_{50}, thus, these parameters are excluded as well. The parameters $H, L_{rep}, tan\alpha$, m, h_{toe}, n, R_c and G_c are excluded from Equation (3.1) as these parameters are controlling the average overtopping discharge but indirectly affect the scouring mechanism. Lastly, as h_0 and t are omitted as it is directly dependent on q_{avg}. After these steps, Equation (3.1) reshapes as Equation (3.2).

$$\varphi\begin{pmatrix} q_{avg} & h_c & d_{50} & x_S & x_A & L_S \\ \sigma & g & \rho_s & L_A & x & z \\ \rho_w & S & A & N & & \end{pmatrix} = 0 \tag{3.2}$$

To form the dimensionless parameters, the π Theorem of Vaschy and Buckingham was applied. Selected independent parameters are ρ_s, g and d_{50}. The dimensionless form of the parameters is presented below.

$$\varphi\begin{pmatrix} \frac{q_{avg}^2}{\Delta g d_{50}^3}, & \frac{h_c}{d_{50}}, & \frac{x_S}{d_{50}}, & \Delta \; or \; \left(\frac{\rho_s}{\rho_w}\right) - 1, & \frac{x_A}{d_{50}}, & \frac{L_S}{d_{50}}, \\ \sigma, & \frac{L_A}{d_{50}}, & \frac{x}{d_{50}}, & \frac{z}{d_{50}}, & \frac{S}{d_{50}}, & \frac{A}{d_{50}} \\ N & & & & & \end{pmatrix} = 0 \tag{3.3}$$

Equation (3.3) contains all the dependent and independent variables. Independent variables are $h_c, \sigma, \Delta, q_{avg}, x, z,$ and N dependent variables are S, A, x_S, x_A, L_S and L_A. The relationship is rewritten in Equation 3.4. Variables in the left matrix are dependent and variables in the right are independent. Mentioned parameters are determined after the physical experiment result data are obtained and investigated.

$$\begin{bmatrix} \frac{S}{d_{50}} & \frac{A}{d_{50}} \\ \frac{x_S}{d_{50}} & \frac{x_A}{d_{50}} \\ \frac{L_S}{d_{50}} & \frac{L_A}{d_{50}} \end{bmatrix} = \varphi\begin{pmatrix} \frac{q_{avg}^2}{\Delta g d_{50}^3}, & \frac{h_c}{d_{50}}, & \Delta \; or \; \left(\frac{\rho_s}{\rho_w}\right) - 1, \\ \sigma, & \frac{x}{d_{50}}, & \frac{z}{d_{50}}, \\ N & & \end{pmatrix} \tag{3.4}$$

3.2 Scaling of the Rubble Mound Revetment

Hughes (1993) states that the Froude model criterion is the most frequently used in hydrodynamic models of coastal engineering problems. The approach has the principle of using gravitational forces to balance inertial forces occurring at the free surface. Froude Number definition is $Fr = V^2/gh$, where V is the water particle velocity, h is the water depth and g is the gravitational acceleration. The principle of the Froude model criterion is Froude number of the model and the Froude number of the prototype must be equal ($Fr_m = Fr_p$). Subscripts m and p represent model and prototype, respectively. To create geometric similarities, length scale (λ_L) is set as $L_m/L_p = \lambda_L$, L represents the parameters in length dimension. Time scale (λ_T) and scale of overtopping (λ_q) per unit have the relations with the length scale as follows, $\lambda_T = \lambda_L^{0.5}$ and $\lambda_q = \lambda_L^{1.5}$. Another issue of scaling the rubble mound structure is the water density effect. This effect occurs because of the differences in densities of water used in the model and the prototype. The water used in the model experiments was fresh water, but the prototype would be subjected to salt water. Dynamic similarity conditions are defined by Hudson et al. (1979) to determine the weight scale (λ_w). For determining the model armor and filter stones, the method of Hudson, is used to solve the density difference of water in the model and prototype. Regarding the viscous effects of the scaled model, the approach, that considers the ratio of the pore velocities for both model and prototype according to the Froude laws, given by Burcharth, Liu, and Troch (1999) was used. The material used in the core is adjusted in diameter to create sufficient wave energy dissipation. The roughness effect of the model armor unit rocks is solved by painting the rocks as in small scale models as Hughes (1993) states unlike the large scale prototypes the surface roughness of the rocks is smaller in models and model roughness may not similitude with the prototype.

Consideration of geometrical and dynamic similarity features, as well as viscous and roughness effects, and properties of the revetment, are given below.

Table 3.1 Properties of Rubble Mound Revetment

Unit Name	$D_{n50,prototype}$ *(meter)*	$D_{n50,model}$ *(centimeter)*	*Stone Class (Prototype – ton)*	*Stone Class (Model – gram)*	n_{model} *(porosity)*
Armor	1.72	4.46	12-15	210-265	0.38
Toe	1.72	4.46	12-15	210-265	0.38
Filter	0.77	1.99	0.4-2	7-35	0.41
Core	0.36	1.30	0.01-0.25	0.4-10	0.41

3.3 Building the Experimental Setup

Experiments are conducted at Middle East Technical University, Civil Engineering Department, Coastal and Ocean Engineering Laboratory wave flume. Wave flume has 1.0 m depth, 26.9 m length, and 6.0 m width. Waves are generated by a single block piston-type wave generator, which is 6.0 m wide, produced by DHI.

Figure 3.2 Wave Generator

The net length of the wave flume that waves can propagate, excluding the 6.3 m of passive wave absorption system, is 20.6 m. In the middle of the flume, there is a 1.5 m wide channel that has window sides for better observation. This channel is separated into two parts having 0.9 m and 0.6 m. The experimental setup is constructed inside the 0.9 m part to reduce the time requirement of leveling and flattening the backfill material and profile measurement time. More than 60 percent of the time was spent on these procedures for a single experiment session so reducing the channel was a necessity. 4.7 m of flat bottom having 0.02 m thickness was

constructed to support the backfill material and rubble mound revetment. In front of the revetment alignment, a 7.2 m long bottom with 0.02 m thickness which has a slope of 1/20 was constructed. The reason that the 1/20 slope is chosen is the fact that to let waves propagate in deep water without any deformation for some time and then let waves deform. Geometric dimensions of the wave flume governed the choice of the length of the slope. The layout plan of the wave flume and experiment setup is presented in Figure 3.4 provided with a cross-sectional view of the locations of the wave gauges that enabled the calibration and measurement of the wave parameters.

Figure 3.3 Perforated Sheet on the Armor Layer of Revetment

After the bottom is constructed, revetment units are placed. Before the armor unit placement, the crown wall is constructed just above the core layer and the wall is stabilized. Armor units are placed into their positions, and they are stabilized with a

square hole perforated sheet which has 2 x 2 cm openings (Figure 3.3). 93 percent of the front area of the armor is open to wave attack.

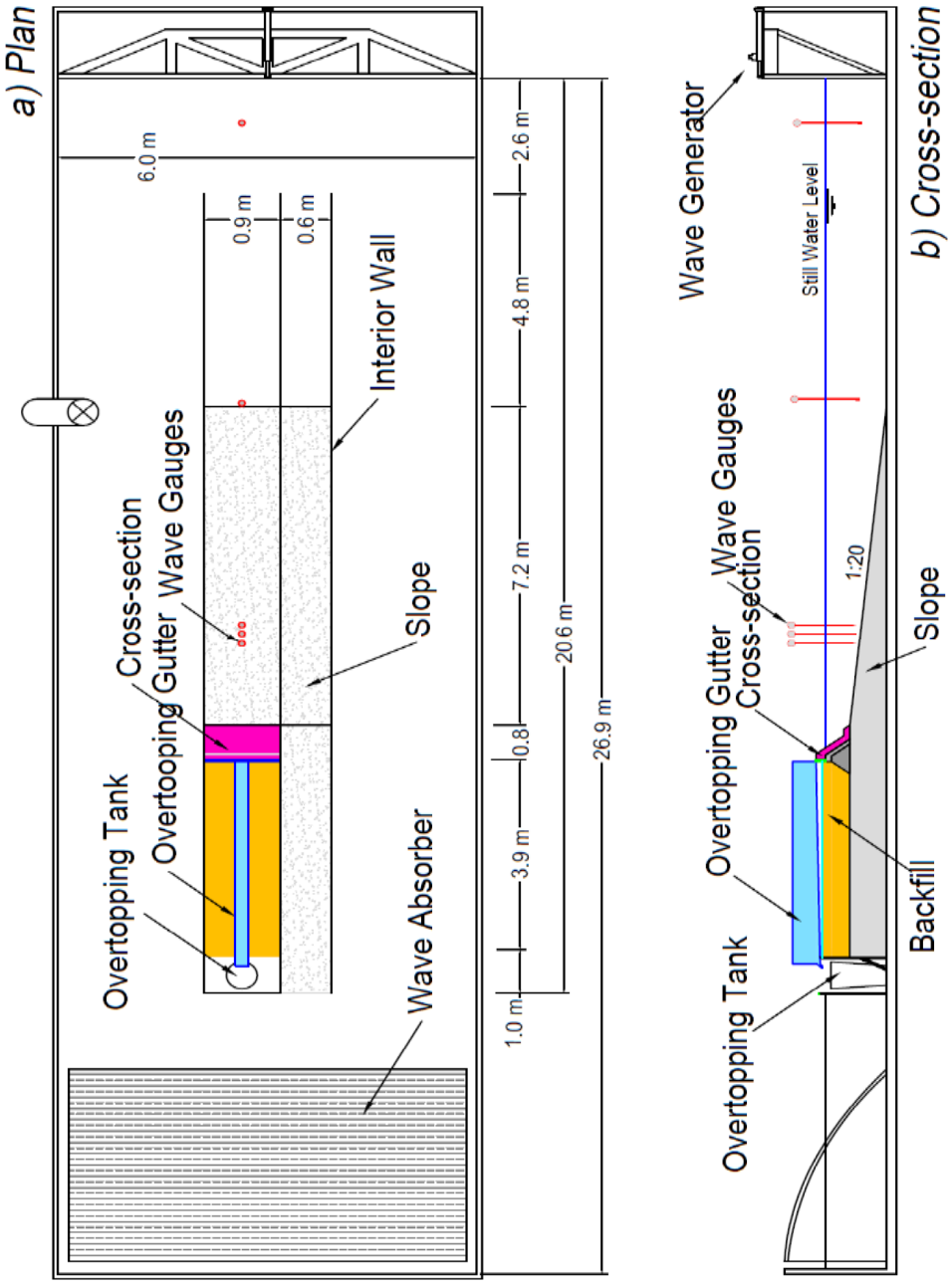

Figure 3.4 Layout Plan of Wave Flume with Experimental Setup (Adopted from Yildirim, 2021)

To prevent any sediment loss from the pores of the revetment or sides of the setup, a water-permeable geotextile filter is placed behind the revetment, under, and sides

of the backfill bed all along. The filter had so small openings that it prevented the escape of the smallest particle of the backfill sediment while enabling the water movement.

Figure 3.5 Placement of the Geotextile Filter

After these procedures, the flume is ready to conduct the experiments. The general view of the flume is given in Figure 3.6.

3.4 Wave Calibration

Wave calibrations are done daily by recording water elevation using DHI-202 type wave gauges of 0.6 m. The sampling frequency was kept at 40 Hz. Before every experiment session, the flume was filled with water at a certain level and one minute of a recording is captured. This process is repeated two more times with different water levels and calibration is done by coupling voltage values with water surface elevation.

Figure 3.6 General View of the Wave Flume and Experimental Setup

3.5 Solitary Wave Generation

In the experiments, solitary waves are used. The waves are generated using a piston-type wave generator. Piston movement and paddle trajectory are based on the

methodology suggested by Malek-Mohammadi and Testik (2010) given in Equation 3.5.

$$\frac{d\xi}{dt} = \sqrt{g\frac{\eta_{wave}}{h_{water}}\left(h_{water}+\frac{\eta_{wave}}{2}\right)\left(\frac{\eta_{wave}}{h_{water}+\eta_{wave}}\right)} \tag{3.5}$$

In equation 3.5, ξ is the trajectory of the paddle, t is time, g is the gravitational acceleration, h_{water} is the water depth and η_{wave} is the wave profile for the solitary wave. The approximate solution for the solitary wave is given in Equation 3.6.

$$\eta_{wave} = H\ sech^2\ [k_{decay}(x-ct)] \tag{3.6}$$

$$k_{decay} = \sqrt{(3H)/(4h_{water}^3)} \tag{3.7}$$

$$c = \sqrt{g\ (h_{water}+H)} \tag{3.8}$$

$$K_s = \frac{1}{h_{water}}\left(\frac{3H}{4h_{water}}\right)^{0.5} \tag{3.9}$$

$$\Omega_s = K_s\ x\ c \tag{3.10}$$

$$T_s = \frac{2\pi}{\Omega_s} \tag{3.11}$$

In equations 3.6, 3.7, and 3.8, H is the height of the solitary wave, k_{decay} is the outskirt decay coefficient, c is the wave celerity, and T_s is the effective period. The paddle trajectory equation is integrated into Boussinesq's Solution and as the result of the piston movement solitary-like waves are generated. When the profile of the generated wave is compared with the theoretical profile of a solitary wave, a slight difference is observed.

Three different solitary-like waves are generated and the comparison of profiles of the solitary waves and theoretical solitary wave profiles of corresponding wave heights are shown in Figure 3.7, Figure 3.8, and Figure 3.9. The profiles of the

solitary-like waves are from the measurements in front of the wave generator paddle as the first of the recorded signal is not affected, i.e. not deformed, from any depth effects.

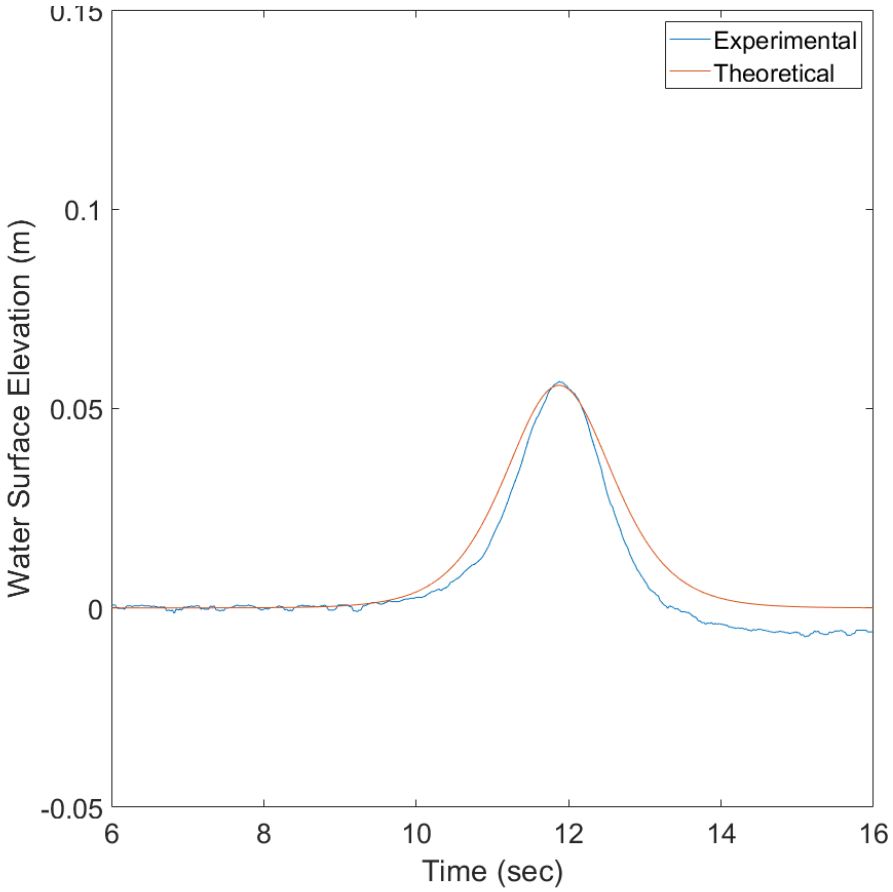

Figure 3.7 Comparison of Experimental Wave vs. Theoretical Solitary Wave Solution – Wave Set 1

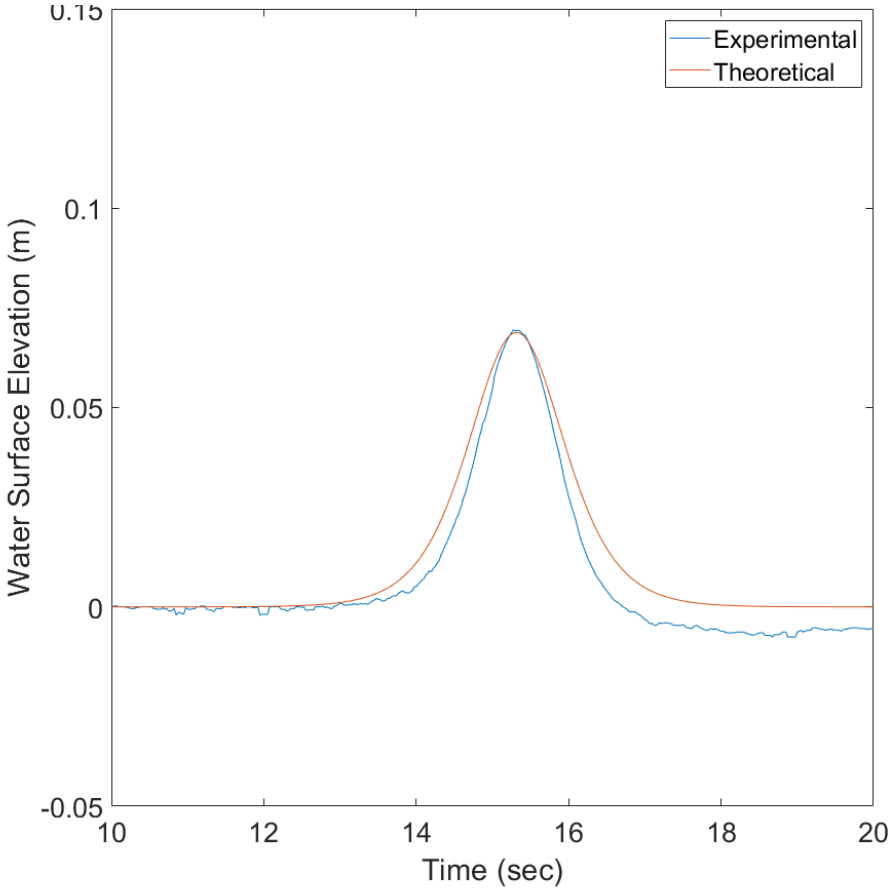

Figure 3.8 Comparison of Experimental Wave vs. Theoretical Solitary Wave Solution – Wave Set 2

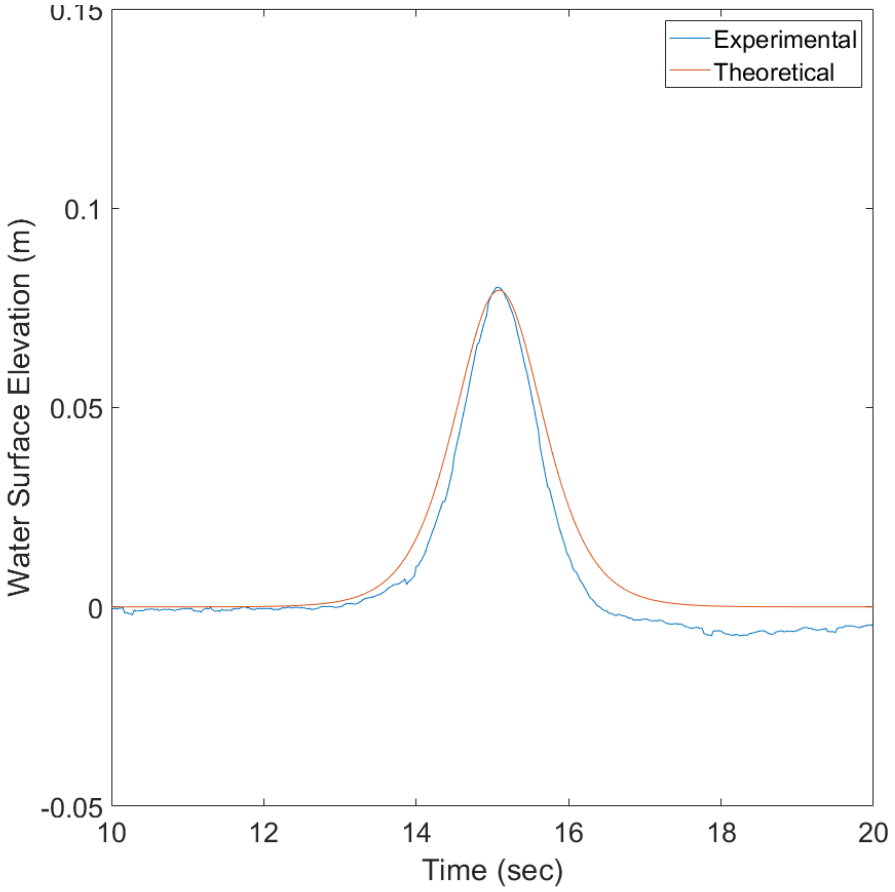

Figure 3.9 Comparison of Experimental Wave vs. Theoretical Solitary Wave Solution – Wave Set 3

Solitary-like waves deformed along the slope as the depth changed along with the propagation of the wave direction. The initial heights and the final heights recorded in front of the revetment are presented in

Table 3.2 Wave Heights of Generated Solitary-like Wave Sets

Wave Set	*H in front of Wave Generator (cm)*	Effective Period of Solitary Wave (s)	*H at Toe of Revetment (cm)*
1	5.58	5.92	8.53
2	6.88	5.28	9.59
3	7.94	4.88	10.15

3.6 Overtopping and Scour Measurements

Wave overtopping volumes are measured by a galvanized steel sheet overtopping gutter which has 25 cm in width. Every solitary wave is sent to attack the revetment 3 times and the mean of the 3 overtopping volumes is taken as the overtopping volume of the related solitary wave.

Figure 3.10 Overtopping Gutter on the Revetment

To convert the overtopping volumes to average overtopping discharges, videos of the overtopping instant of the waves are captured at 5 different points on the crown wall (Figure 4.1). From the same videos, jet thickness is measured with an accuracy

of 1 mm. The camera used to capture the videos is Sony RX0 Mark II. The touch of the overtopping wave to the crown wall is accepted as the flow start time and the time the flow stopped over the crown wall is accepted as the end time of the jet flow. The difference between the start and end time of the jet flow is jet flow duration and by dividing overtopping volume by jet flow duration, average overtopping discharge values are calculated.

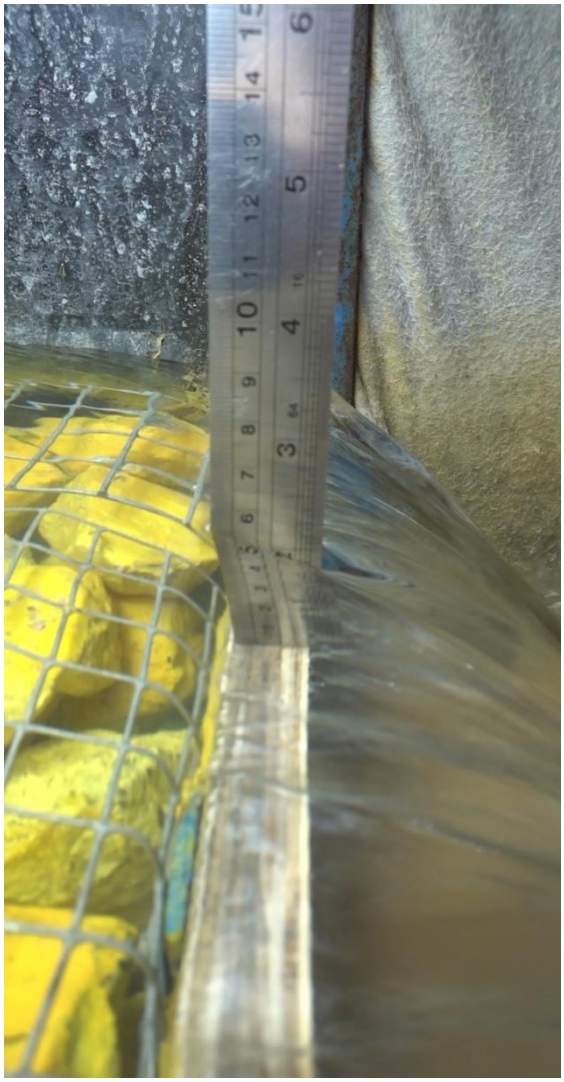

Figure 3.11 A Screenshot from Flow Thickness and Duration Measurement Videos

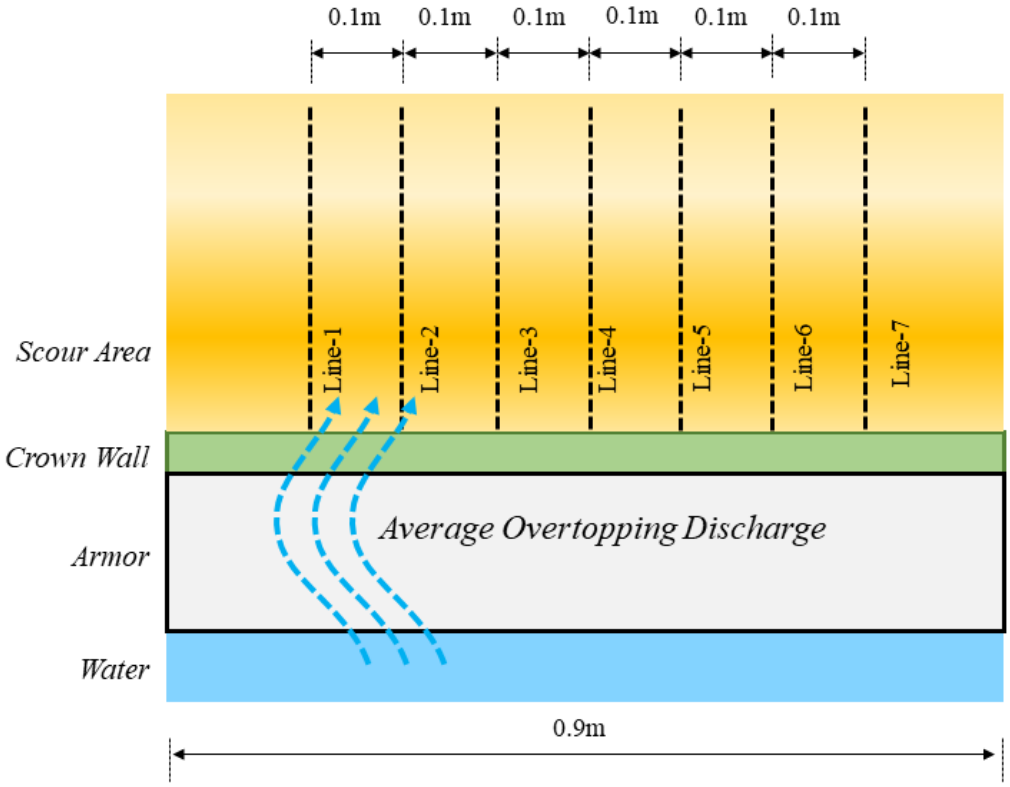

Figure 3.12 Lazer Point Lines of Scour Measurements

Backfill material is placed in its place and a smooth surface is created by compacting the backfill area while it is flooded. The reason for compaction in the flooded phase is to achieve a smooth surface by distributing the grains on the surface by their natural settling velocity. After a smooth surface is observed underwater, the water is drained slowly without letting it disturb the surface profile until the experiment water level is achieved.

The laser sensor used in the system to take vertical measurements is the Banner® brand LTF24IC2LDQ model. Its accuracy is below 0.3 mm. In Figure 3.12, the measurement lines that the laser has followed are presented. Measurements are taken for every 1 cm on a line. 10 cm gaps are placed between the lines and measurements of 7 different lines are taken and the average of the 7 lines are accepted as the scour depth to present scour evolution in a two-dimensional form. In Figure 3.13, it is shown that the mean of all 7 lines of measurement is representative of the scour formation, and the differences between the individual measurements of laser line paths are close to

each other. For the respective test, absolute percentage errors of each individual line measurement are, 0.047, 0.023, 0.014, 0.011, 0.028, 0.050, 0.11 and the mean of the errors is 0.04. The backfill area is let drain after every wave attack. In a real-life scenario, this would not be the case where the complete drainage is satisfied but, in the laboratory environment, we had to wait for the water body in the wave flume to be settled down to generate solitary waves without any disturbance.

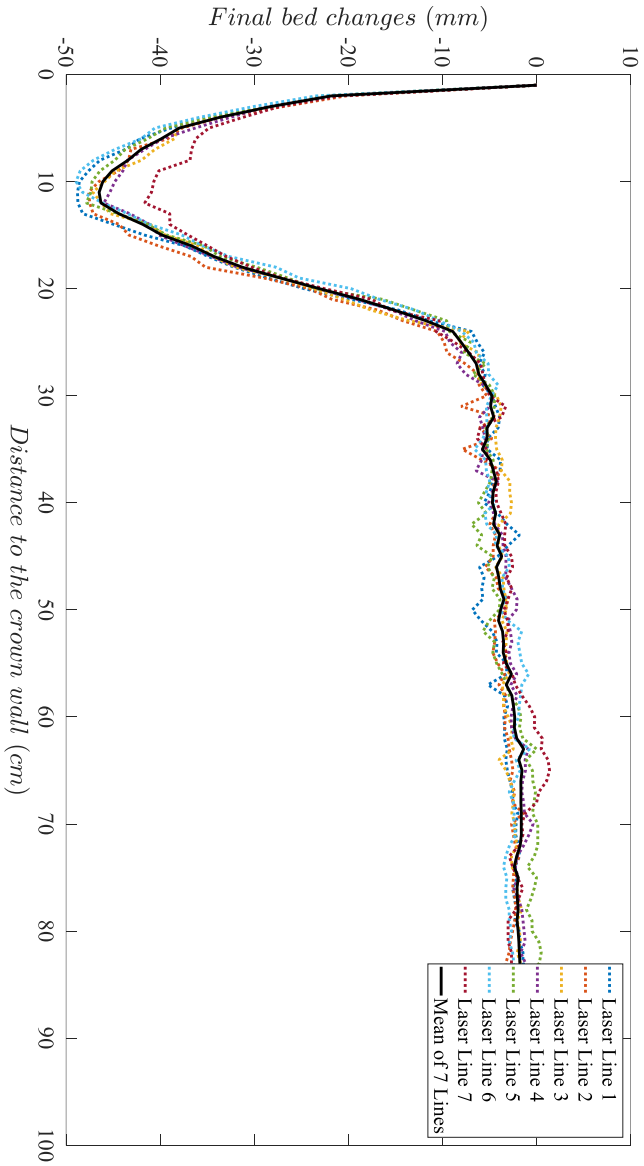

Figure 3.13 Laser Line Measurements and Mean of the Measurements for Test 1

CHAPTER 4

RESULTS

4.1 Overtopping Results

As mentioned in the methodology, overtopping of the solitary waves is measured by a 25 cm wide gutter. Volumes that overtopped the revetment and gathered with the gutter are presented in Table 4.1.

Table 4.1 Overtopped Volume of Solitary-like Waves (l)

Wave Set	*Wave No.*	*Volume (l)*	*Mean Volume (l)*
Set-1	DA-1.1	5.00	4.97
	DA-1.2	4.90	
	DA-1.3	5.00	
Set-2	DA-2.1	7.35	7.25
	DA-2.2	7.25	
	DA-2.3	7.15	
Set-3	DA-3.1	8.75	8.77
	DA-3.2	8.75	
	DA-3.3	8.80	

The average of three waves in a set is accepted as the overtopping volume of the related solitary-like wave. The overflow jet thickness measurements and overtopping duration tests carried out for Set-1, Set-2, and Set-3 solitary waves for 5 different points each, are presented in Table 4.2 and it is observed that as the wave height increases, overtopped volume of the wave is increased as well.

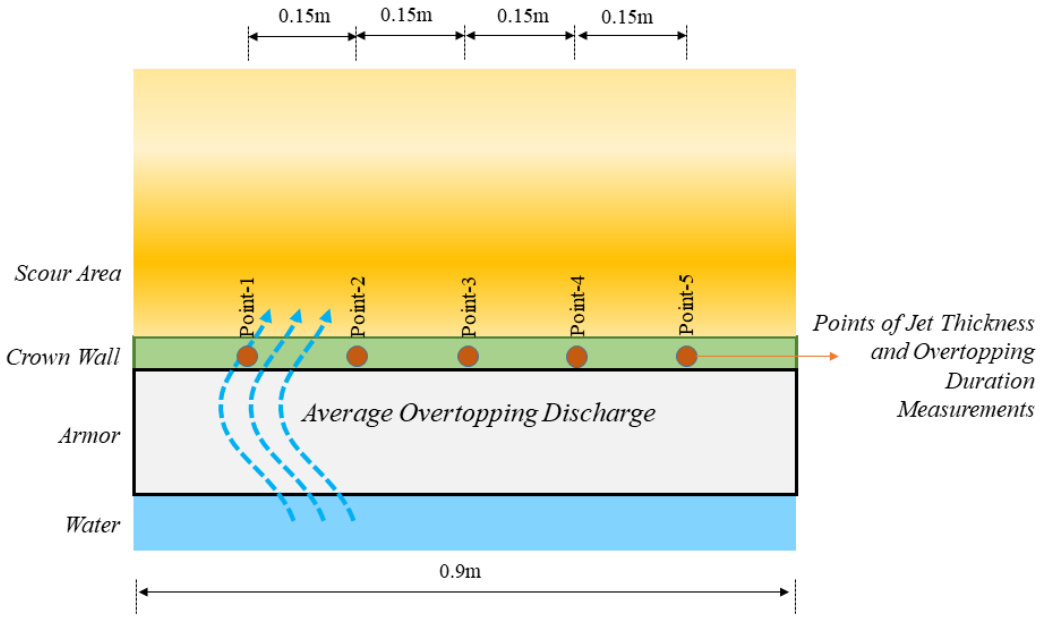

Figure 4.1 Points of Jet Thickness and Overtopping Duration Measurements

Table 4.2 Durations and Jet Thicknesses Measured During Overtopping Process

Wave Set	*Point*	*Duration of Overtopping (sec)*	*Jet Thickness (cm)*	*Average Overtopping Duration (sec)*	*Average Jet Thickness (cm)*
Set-1	*1*	1.57	4.30	1.70	4.26
	2	1.60	4.50		
	3	1.69	4.20		
	4	1.80	4.00		
	5	1.82	4.30		
Set-2	*1*	1.82	5.20	1.76	4.98
	2	1.81	5.00		
	3	1.75	4.70		
	4	1.74	5.00		
	5	1.68	5.00		
Set-3	*1*	1.82	5.70	1.81	5.60
	2	1.82	5.70		
	3	1.77	5.40		
	4	1.83	5.50		
	5	1.83	5.70		

From Table 4.1, using the volume of overtopped water and from Table 4.2, durations of overtopping flow, the average overtopping discharge for the generated wave sets are determined and presented in Table 4.3.

Table 4.3 Wave Heights of Generated Solitary-like Wave Sets

Wave Set	*Average Overtopping Discharge (l/sec)*
Set 1	11.73
Set 2	16.48
Set 3	19.35

4.2 Scour Experiment Results

For scour experiments, 18 different combinations of H_{toe}, d_{50}, h_c and N are used and resulted. For each combination of H_{toe}, d_{50} and h_c, scour profile evolutions are observed. After the scour profiles are determined, multiple regression analysis is conducted to analyze the effects of parameters on maximum scour depth and predict the maximum scour depth depending on the parameters of combination used.

Table 4.4 Tests Conducted and Related Parameters

Test No.	d_{50} *(m)*	h_c *(m)*	H_{toe} *(m)*	*Number of Experiments Conducted*	*Number of Measurements*
1	0.00021	0.03	0.086	10	6
2	0.00021	0.03	0.096	10	5
3	0.00021	0.03	0.102	10	8
4	0.00021	0.06	0.086	10	3
5	0.00021	0.06	0.096	10	3
6	0.00021	0.06	0.102	10	3
7	0.00066	0.00	0.086	10	6
8	0.00066	0.00	0.096	10	6
9	0.00066	0.00	0.102	10	6
10	0.00066	0.03	0.086	10	5

Table 4.4 (continued)

11	0.00066	0.03	0.096	10	5
12	0.00066	0.03	0.102	10	5
13	0.00066	0.06	0.086	10	5
14	0.00066	0.06	0.096	10	5
15	0.00066	0.06	0.102	10	5
16	0.00335	0.03	0.086	3	3
17	0.00335	0.03	0.096	3	3
18	0.00335	0.03	0.102	3	3

Maximum scour depths measured at the rear side of revetment due to solitary-like wave overtopping for each experiment are presented in Table 4.5. In total, 85 experiments are conducted.

Table 4.5 Maximum Scour Depths at Rear Side of Revetment

Test No.	d_{50} *(m)*	h_c *(m)*	H_{toe} *(m)*	*N*	q_{avg}*(lt/s/m)*	*S (m)*
Test1-W1	0.00021	0.03	0.086	1	11.73	0.0049
Test1-W2	0.00021	0.03	0.086	2	11.73	0.0106
Test1-W3	0.00021	0.031	0.086	3	11.73	0.0166
Test1-W5	0.00021	0.03	0.086	5	11.73	0.0266
Test1-W7	0.00021	0.03	0.086	7	11.73	0.0347
Test1-W10	0.00021	0.03	0.086	10	11.73	0.0465
Test2-W1	0.00021	0.03	0.096	1	16.48	0.0061
Test2-W2	0.00021	0.03	0.096	2	16.48	0.0112
Test2-W3	0.00021	0.03	0.096	3	16.48	0.0164
Test2-W5	0.00021	0.03	0.096	5	16.48	0.0256
Test2-W10	0.00021	0.03	0.096	10	16.48	0.0409
Test3-W1	0.00021	0.03	0.102	1	19.35	0.0072
Test3-W2	0.00021	0.03	0.102	2	19.35	0.0105

Table 4.5 (continued)

Test No.	d_{50} *(m)*	h_c *(m)*	H_{toe} *(m)*	*N*	q_{avg}*(lt/s/m)*	*S (m)*
Test3-W3	0.00021	0.03	0.102	3	19.35	0.0145
Test3-W4	0.00021	0.03	0.102	4	19.35	0.0190
Test3-W5	0.00021	0.03	0.102	5	19.35	0.0246
Test3-W6	0.00021	0.03	0.102	6	19.35	0.0292
Test3-W7	0.00021	0.03	0.102	7	19.35	0.0350
Test3-W10	0.00021	0.03	0.102	10	19.35	0.0452
Test4-W1	0.00021	0.06	0.086	1	11.73	0.0118
Test4-W2	0.00021	0.06	0.086	2	11.73	0.0196
Test4-W3	0.00021	0.06	0.086	3	11.73	0.0260
Test5-W1	0.00021	0.06	0.096	1	16.48	0.0111
Test5-W2	0.00021	0.06	0.096	2	16.48	0.0191
Test5-W3	0.00021	0.06	0.096	3	16.48	0.0254
Test6-W1	0.00021	0.06	0.102	1	19.35	0.0142
Test6-W2	0.00021	0.06	0.102	2	19.35	0.0226
Test6-W3	0.00021	0.06	0.102	3	19.35	0.0286
Test7-W1	0.00066	0	0.086	1	11.73	0.0006
Test7-W2	0.00066	0	0.086	2	11.73	0.0037
Test7-W3	0.00066	0	0.086	3	11.73	0.0073
Test7-W5	0.00066	0	0.086	5	11.73	0.0142
Test7-W7	0.00066	0	0.086	7	11.73	0.0214
Test7-W10	0.00066	0	0.086	10	11.73	0.0324
Test8-W1	0.00066	0	0.096	1	16.48	0.0018
Test8-W2	0.00066	0	0.096	2	16.48	0.0057
Test8-W3	0.00066	0	0.096	3	16.48	0.0089
Test8-W5	0.00066	0	0.096	5	16.48	0.0168
Test8-W7	0.00066	0	0.096	7	16.48	0.0251
Test8-W10	0.00066	0	0.096	10	16.48	0.0370
Test9-W1	0.00066	0	0.102	1	19.35	0.0025
Test9-W2	0.00066	0	0.102	2	19.35	0.0064

Table 4.5 (continued)

Test No.	d_{50} *(m)*	h_c *(m)*	H_{toe} *(m)*	*N*	q_{avg}*(lt/s/m)*	*S (m)*
Test9-W3	0.00066	0	0.102	3	19.35	0.0095
Test9-W5	0.00066	0	0.102	5	19.35	0.0162
Test9-W7	0.00066	0	0.102	7	19.35	0.0249
Test9-W10	0.00066	0	0.102	10	19.35	0.0380
Test10-W1	0.00066	0.03	0.086	1	11.73	0.0050
Test10-W2	0.00066	0.03	0.086	2	11.73	0.0120
Test10-W3	0.00066	0.03	0.086	3	11.73	0.0180
Test10-W5	0.00066	0.03	0.086	5	11.73	0.0303
Test10-W10	0.00066	0.03	0.086	10	11.73	0.0521
Test11-W1	0.00066	0.03	0.096	1	16.48	0.0056
Test11-W2	0.00066	0.03	0.096	2	16.48	0.0126
Test11-W3	0.00066	0.03	0.096	3	16.48	0.0184
Test11-W5	0.00066	0.03	0.096	5	16.48	0.0294
Test11-W10	0.00066	0.03	0.096	10	16.48	0.0534
Test12-W1	0.00066	0.03	0.102	1	19.35	0.0073
Test12-W2	0.00066	0.03	0.102	2	19.35	0.0146
Test12-W3	0.00066	0.03	0.102	3	19.35	0.0220
Test12-W5	0.00066	0.03	0.102	5	19.35	0.0336
Test12-W10	0.00066	0.03	0.102	10	19.35	0.0568
Test13-W1	0.00066	0.06	0.086	1	11.73	0.0118
Test13-W2	0.00066	0.06	0.086	2	11.73	0.0170
Test13-W3	0.00066	0.06	0.086	3	11.73	0.0233
Test13-W5	0.00066	0.06	0.086	5	11.73	0.0302
Test13-W10	0.00066	0.06	0.086	10	11.73	0.0517
Test14-W1	0.00066	0.06	0.096	1	16.48	0.0130
Test14-W2	0.00066	0.06	0.096	2	16.48	0.0194
Test14-W3	0.00066	0.06	0.096	3	16.48	0.0263
Test14-W5	0.00066	0.06	0.096	5	16.48	0.0336
Test14-W10	0.00066	0.06	0.096	10	16.48	0.0564

Table 4.5 (continued)

Test No.	d_{50} *(m)*	h_c *(m)*	H_{toe} *(m)*	*N*	q_{avg}*(lt/s/m)*	*S (m)*
Test15-W1	0.00066	0.06	0.102	1	19.35	0.0112
Test15-W2	0.00066	0.06	0.102	2	19.35	0.0172
Test15-W3	0.00066	0.06	0.102	3	19.35	0.0230
Test15-W5	0.00066	0.06	0.102	5	19.35	0.0347
Test15-W10	0.00066	0.06	0.102	10	19.35	0.0508
Test16-W1	0.00335	0.03	0.086	1	11.73	0.0102
Test16-W2	0.00335	0.03	0.086	2	11.73	0.0133
Test16-W3	0.00335	0.03	0.086	3	11.73	0.0160
Test17-W1	0.00335	0.03	0.096	1	16.48	0.0123
Test17-W2	0.00335	0.03	0.096	2	16.48	0.0169
Test17-W3	0.00335	0.03	0.096	3	16.48	0.0218
Test18-W1	0.00335	0.03	0.102	1	19.35	0.0182
Test18-W2	0.00335	0.03	0.102	2	19.35	0.0230
Test18-W3	0.00335	0.03	0.102	3	19.35	0.0342

From Table 4.5 it can be concluded that maximum scour depth for the first few wave attacks increased gradually. It can be said that with a proper amount of wave attacks, an equilibrium stage may be reached for the backfill scouring but it is not in the scope of this study. In Figure 4.2, it can be observed that the scour slope gets milder after every wave attack. The normalization of the scour depth is done by dividing the scour measurements to the maximum scour depth to investigate ΔS relation with N.

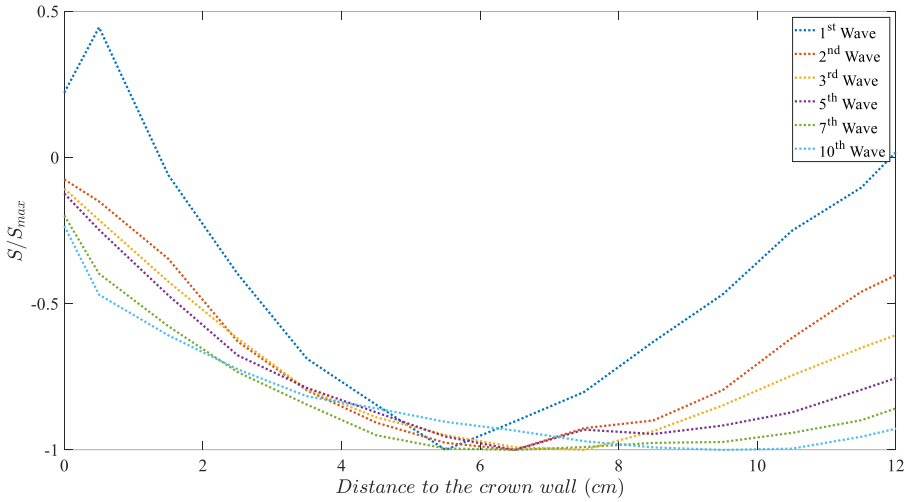

Figure 4.2 Normalized Scour Depth vs Distance to the Crown Wall for Test 1

4.2.1 Scour Profile Evolution

Rear side profiles of revetment are measured after wave attacks and the evolution of scour profiles is observed in every test. In Figure 4.3, scour profile measurements for different wave attacks in Test 1 are presented.

From the observations, it is seen that scour hole is generated near the crown wall except in a few cases where scour hole has occurred just next to the crown wall. The reason behind this unexpected occurrence is that the wave pressure exceeds a limit and resulting in the rear side movement.

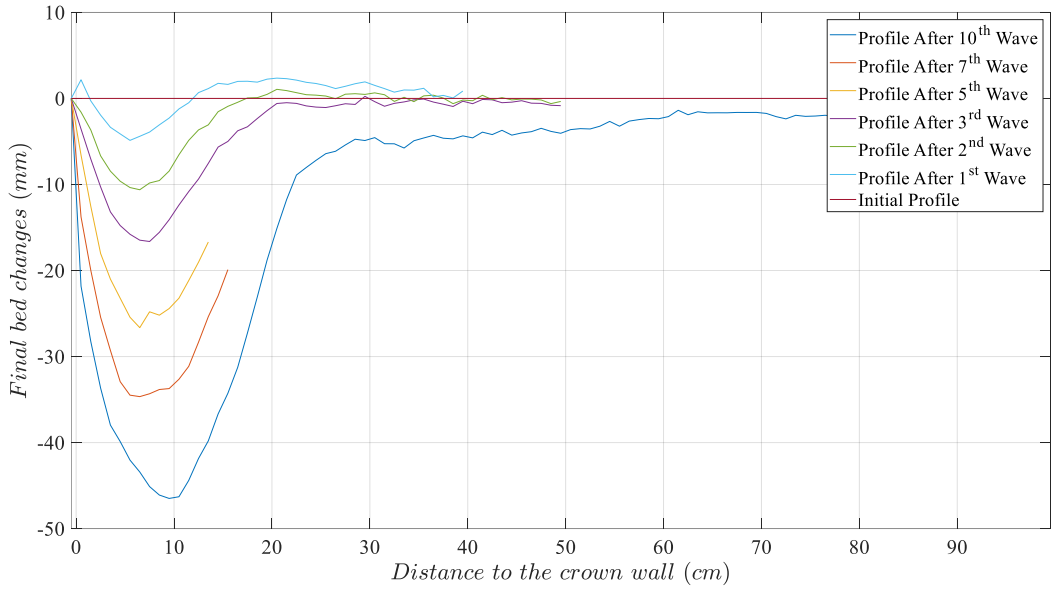

Figure 4.3 Scour Profile Evolution of Test 1

4.2.2 Multiple Regression Analysis

Results of rear side scour profiles are investigated, and the most effective parameters of the scouring mechanism are found as q_{avg}, h_c and N. Linear regression analysis is conducted and not a robust relation is found between dependent and independent variables. The investigation is continued with logarithmic regression analysis and the results are found in better agreement. The relationship between dimensionless scour depth and effective parameters are presented in Figure 4.4, Figure 4.5, and Figure 4.6. Multiple regression analysis is conducted in IBM SPSS Statistics Software.

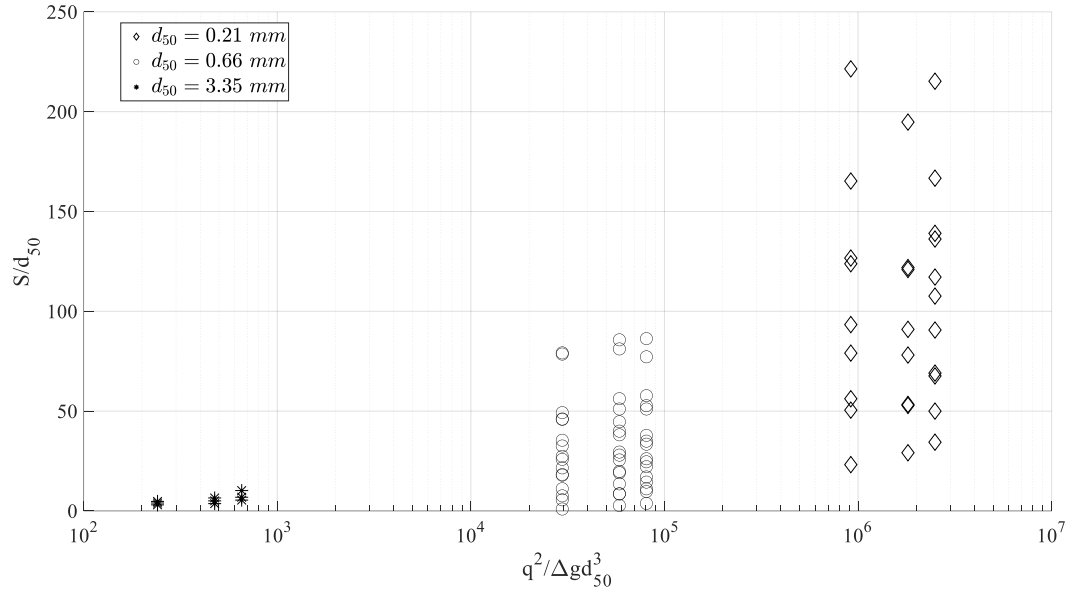

Figure 4.4 Relationship Between the Dimensionless Scour Depth and Dimensionless Discharge

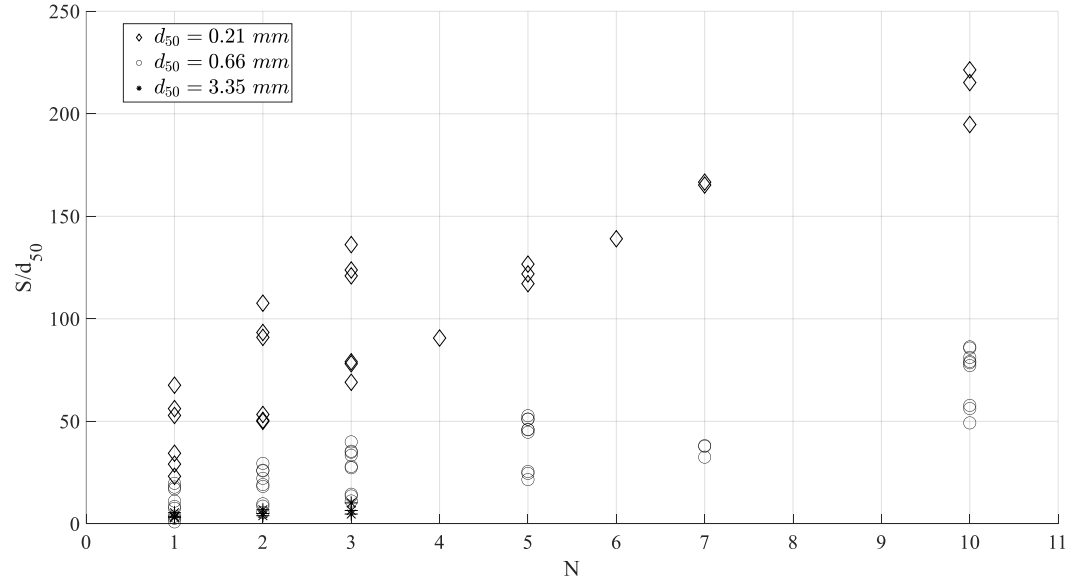

Figure 4.5 Relationship Between the Dimensionless Scour Depth and Wave Count

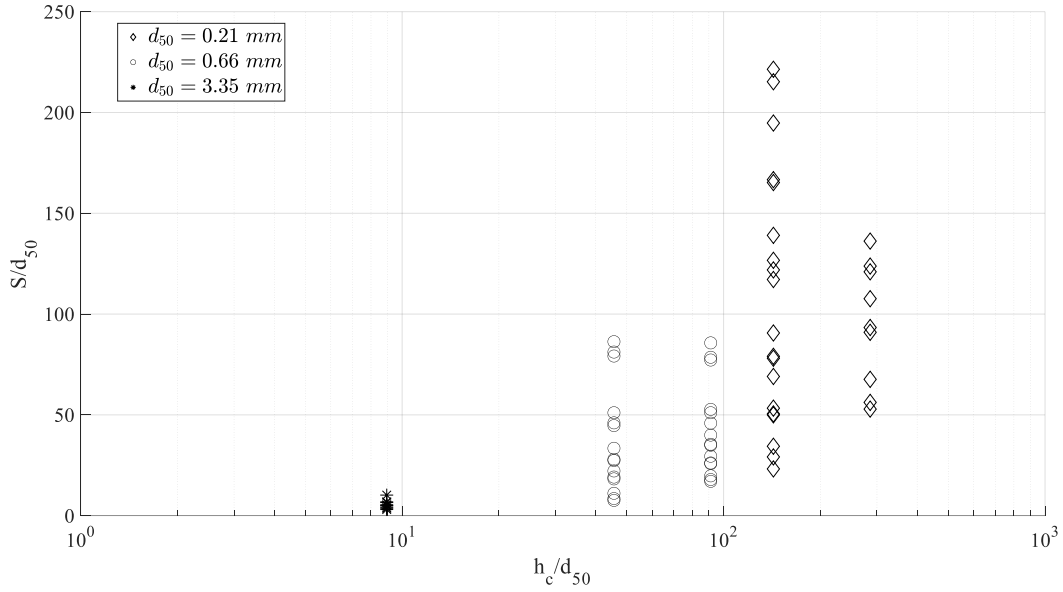

Figure 4.6 Relationship Between the Dimensionless Scour Depth and Dimensionless Backfill Height

From Figure 4.4, Figure 4.5, and Figure 4.6 it is observed that dimensionless scour depth is highly correlated with the dimensionless average overtopping discharge, dimensionless backfill height, and wave count. The R^2 values for Figure 4.4, Figure 4.5, and Figure 4.6 are found as 0.40, 0.36, and 0.32, respectively.

Table 4.6 Coefficients Determined by Multi Regression Analysis

Dependent Parameter	Independent Parameters	B	Std. Error	Beta	R-Square
$\frac{S}{d_{50}}$	$Constant$	-0.759	0.102	-	0.973
	$\frac{q_{avg}^2}{\Delta g d_{50}^3}$	0.132	0.023	0.334	
	$\frac{h_c}{d_{50}}$	0.483	0.062	0.449	
	N	0.763	0.031	0.524	

In Table 4.6, coefficients determined from multi regression analysis are presented. It is noted that standard errors for the independent variables are low and the R-Square of the multi regression analysis is 0.973 which implies that the correlation is highly positive. In the results, unstandardized coefficients are used as independent variables

are measured in their original scales i.e, the same units which are taken from the source to train the model. Beta values show the degree of change in the outcome of dimensionless scour prediction. N has the highest beta value thus, it is the most effective parameter for maximum scour depth. Backfill depth is the second most effective parameter meaning that the velocity gained by water while falling from the crown wall to the backfill has a higher effect than the overtopping discharge in the experiments conducted.

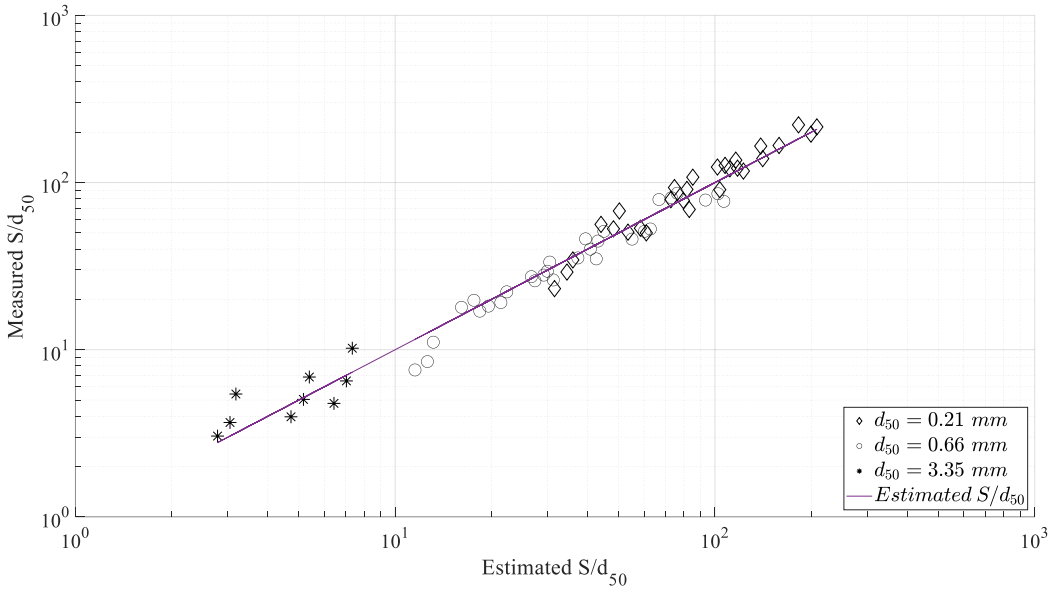

Figure 4.7 Correlation of Estimated Dimensionless Scour Depth with Measured Dimensionless Scour Depth

The results of multi regression analysis are used to derive an equation to predict the maximum dimensionless scour depth with parameters of dimensionless average overtopping discharge, dimensionless backfill depth, and wave count. In Equation (4.1) general formula for the prediction formula of dimensionless scour depth is given. In Equation (4.2) the coefficients are placed and the final form of the equation is derived. The valid range of the equation is, $0.96 < \frac{S}{d_{50}} < 371$, $241 < \frac{q_{avg}^2}{\Delta g d_{50}^3} < 250000$, $0 < \frac{h_c}{d_{50}} < 286$ and $1 \leq N \leq 10$.

$$\frac{S}{d_{50}} = \exp(B) \left(\frac{q_{avg}^2}{\Delta g d_{50}^3}\right)^A \left(\frac{h_c}{d_{50}}\right)^C N^D \tag{4.1}$$

$$\frac{S}{d_{50}} = 0.468 \left(\frac{q_{avg}^2}{\Delta g d_{50}^3}\right)^{0.132} \left(\frac{h_c}{d_{50}}\right)^{0.483} N^{0.763} \tag{4.2}$$

CHAPTER 5

DISCUSSION AND CONCLUSIONS

In this chapter, the discussions on the results of the physical experiments and conclusions are presented. Firstly, one of the primary research questions of the study is to investigate how different wave conditions affect the scour at the rear side under the same structural and morphological conditions. It was seen in the experiments that average overtopping discharge is directly related to solitary wave height at the same depth. Furthermore, it is observed that scour increases when the average overtopping discharge is increased. Moreover, in terms of the shape of the scour profiles, the first few attacking waves show similar scour profiles at the rear side of the coastal revetment.

In the, it is observed that the depth of the scour hole varies with overflow discharge, grain size diameter, and backfill depth. During the experimental studies, it is seen that the overflow discharge is directly dependent on the solitary-like wave height. As a result, when the wave height is increased, the overflow discharge is increased. Furthermore, scour hole depth and overflow height are also a direct correlation. Therefore, scour hole depth is increased as the overflow discharge and wave height are increased. Another parameter is determined as the median grain size diameter of the backfill material. For the loose sand, it is seen that the scour depth is increased with increasing grain size diameter since the sediment transport rates are directly related to the grain size. This applies to the gravel backfill with the heights median diameter of sediment used in the physical experiments. Even though the scour depth is higher for the increased median diameter, it is noted that the number of sediment grains that are moved decreases as the grain size diameter increases. Finally, it is observed that the backfill depth is an effective physical property for the scouring mechanism. As the backfill depth is increased, the depth of the scour hole is increased since the overtopped water volume hits the backfill material with higher

vertical velocities. Therefore, it applies higher impact pressures on the sediment at the rear side, which results in deeper scour depths.

Regarding the relation between the number of overtopped waves and the scour profiles, it is investigated that the scour depths are gradually increasing with the increasing number of overtopped solitary waves. On the other hand, the shapes of the scour profiles for Test 4-5-6 and, Test 13-14-15 are deformed after the attack of the first few waves on the coastal revetment. In the experiments, the reason behind this issue is visually observed. It must be noted that these tests have a common parameter which is h_c and for these experiments h_c is 0.06 m. As the backfill material at the rear side of the structure is eroded, the wave pressure under the crown wall resulted in a motion of the sediment which lies near the crown wall. Therefore, for the regarding experiments, the shapes of the scour profiles are deformed.

In the results section, it is noted that the most effective parameters of the scouring mechanism are q_{avg}, h_c and N for this study. The result of multiple regression analysis is visualized in the figure below and shows the compatibility of the predicted equation for the dimensionless scour depth with measured dimensionless scour depths.

In this study, the results of physical experiments are limited to the maximum scour depth at the rear side of the revetment. The reason behind this limitation is that the rear side section is not long enough to observe and measure the total scour length and accretion process. The flow due to the overtopping of solitary-like waves is partly absorbed by the rear side sediment and partly escaped the rear side at the end. In further research, it is possible to observe and measure the scour length, accretion height, and accretion zone length in detail with a rear side of proper length.

This study shows that there is a strong correlation between scour depth and selected independent parameters for the same structural conditions such as crest width, crown wall type, structure front slope, solitary wave shape, grain sizes, and compaction of backfill material. Research on this topic may be extended for different structural

conditions to derive a generic formula to predict maximum scour depth at the rear side of a rubble mound revetment.

REFERENCES

Bricker, Jeremy D., Mathew Francis, and Akihiko Nakayama. 2012. "Scour Depths near Coastal Structures Due to the 2011 Tohoku Tsunami." *Journal of Hydraulic Research* 50(6): 637–41.

Burcharth, Hans F, Zhou Liu, and Peter Troch. 1999. "Scaling of Core Material in Rubble Mound Breakwater Model Tests." *COPEDEC V*.

Chen, Jie et al. 2013. "Tsunami-Induced Scour at Coastal Roadways: A Laboratory Study." *Natural Hazards* 69(1): 655–74.

Chen, Jie, Changbo Jiang, Wu Yang, and Guizhen Xiao. 2016. "Laboratory Study on Protection of Tsunami-Induced Scour by Offshore Breakwaters." *Natural Hazards* 81(2): 1229–47.

Chiew, Yee-Meng;, Siow-Yong; Lim, and Cheng. 2004. *Mechanisms Of Scour Induced By Tsunami Runup*. Nian-Sheng (Hg. https://hdl.handle.net/20.500.11970/99932.

Hsiao, Shih Chun, and Ting Chieh Lin. 2010. "Tsunami-like Solitary Waves Impinging and Overtopping an Impermeable Seawall: Experiment and RANS Modeling." *Coastal Engineering* 57(1): 1–18.

Huang, Ching-Jer, and Chih-Ming Dong. 2001. 43 Coastal Engineering *On the Interaction of a Solitary Wave and a Submerged Dike*. www.elsevier.comrlocatercoastaleng.

Hudson, Robert Y et al. 1979. *Coastal Hydraulic Models*.

Hughes, Steven A. 1993. *Physical Models and Laboratory Techniques in Coastal Engineering*. World Scientific.

International Society of Offshore and Polar Engineers. 2008. *The Proceedings of the Eighteenth (2008) International Offshore and Polar Engineering Conference :*

Vancouver, Canada, July 6-11, 2008 : ISOPE-2008 Vancouver. International Society of Offshore and Polar Engineers.

Jayaratne, Mantripathi Prabath Ravindra et al. 2016. "Failure Mechanisms and Local Scour at Coastal Structures Induced by Tsunami." *Coastal Engineering Journal* 58(4).

Jiang, Changbo et al. 2017. "Numerical Investigation of Tsunami-Like Solitary Wave Interaction with a Seawall." In *Journal of Earthquake and Tsunami*, World Scientific Publishing Co. Pte Ltd.

Kato, Fuminori et al. 2001. "The Grain-Size Effects on Scour around a Cylinder Due to Tsunami Run-Up." In *ITS*,.

Kato, Fuminori, Yoshio Suwa, Kunihiro Watanabe, and Satoshi Hatogai. 2012. "MECHANISMS OF COASTAL DIKE FAILURE INDUCED BY THE GREAT EAST JAPAN EARTHQUAKE TSUNAMI." *Coastal Engineering*.

Kobayashi, Nobuhisa, and Andrew R. Lawrence. 2004. "Cross-Shore Sediment Transport under Breaking Solitary Waves." *Journal of Geophysical Research: Oceans* 109(3).

Larsen, Bjarke Eltard et al. 2018. "Experimental Study of Tsunami-Induced Scour around a Monopile Foundation." *Coastal Engineering* 138: 9–21.

Liu, Chang-Gen (~j-~, and Jian-Hua Tao. 2004. 25 Applied Mathematics and Mechanics (English Edition *MODELING THE INTERACTION OF SOLITARY WAVES AND SEMI-CIRCULAR BREAKWATERS BY USING UNSTEADY REYNOLDS EQUATIONS**.

Malek-Mohammadi, Siamak, and Firat Y Testik. 2010. *New Methodology for Laboratory Generation of Solitary Waves*.

McGovern, D. J. et al. 2019. "Experimental Observations of Tsunami Induced Scour at Onshore Structures." *Coastal Engineering* 152.

Mcgovern, David ;, Tiziana ; Rossetto, and David Todd. 2019. “Tsunami Scour and Forces at Onshore Structures.” https://doi.org/10.18451/978-3-939230-64-9_051.

Nakamura, T, ; Y Nezasa, ; N Mizutani, and Y Kotake. 2015. *Study on Tsunami Scour at the Landward Toe of a Coastal Dike and the Tsunami Force on Its Armor Blocks*.

Nakamura, Tomoaki, Yasuki Kuramitsu, and Norimi Mizutani. 2008. *TSUNAMI-INDUCED LOCAL SCOUR AROUND A SQUARE STRUCTURE*.

Okura, Shota, and Tetsuya Hiraishi. 2018. “Experimental Study on Scouring of Land behind Seawall Due to Overflowing Tsunami.” In *Journal of Coastal Research*, Coastal Education Research Foundation Inc., 821–25.

Rahman, Md Abedur, Norio Tanaka, and Nijati Reheman. 2021. “Experimental Study on Reduction of Scouring and Tsunami Energy through a Defense System Consisting a Seaward Embankment Followed by Vertically Double Layered Vegetation.” *Ocean Engineering* 234.

Tanaka, Norio, and Masayuki Sato. 2015. “Scoured Depth and Length of Pools and Ditches Generated by Overtopping Flow from Embankments during the 2011 Great East Japan Tsunami.” *Ocean Engineering* 109: 72–82.

Tsai, Ching Piao, Ying Chi Chen, Chun Jen Chen, and Chang Lin. 2016. “Simulation of the Effect of Breakwater on the Propagation of Solitary Waves.” *Journal of Marine Science and Technology (Taiwan)* 24(4): 780–89.

Wang, Dong, Taro Arikawa, Shaowu Li, and Hayao Gen. 2015a. *Coastal Structures and Solutions to Coastal Disasters 2015 Numerical Simulation on Scour behind Seawalls Due to Tsunami Overflow*.

Coastal Structures and Solutions to Coastal Disasters 2015 Numerical Simulation on Scour behind Seawalls Due to Tsunami Overflow.

Xiao, Heng, Yin Lu Young, and Jean H. Prévost. 2010. “Hydro- and Morpho-Dynamic Modeling of Breaking Solitary Waves over a Fine Sand Beach. Part II: Numerical Simulation.” *Marine Geology* 269(3–4): 119–31.

Xu, Conghao, Zhenhua Huang, and Yu Yao. 2019. “A Wave-Flume Study of Scour at a Pile Breakwater: Solitary Waves.” *Applied Ocean Research* 82: 89–108.

Yildirim, Mehmet Emre. 2021. “SCOUR AT THE REAR SIDE OF RUBBLE MOUND REVETMENTS.”

Young, D. Morgan, and Firat Y. Testik. 2009. “Onshore Scour Characteristics around Submerged Vertical and Semicircular Breakwaters.” *Coastal Engineering* 56(8): 868–75.

APPENDICES

A. Rear Side Scour Formations for $d_{50} = 0.21\ mm$

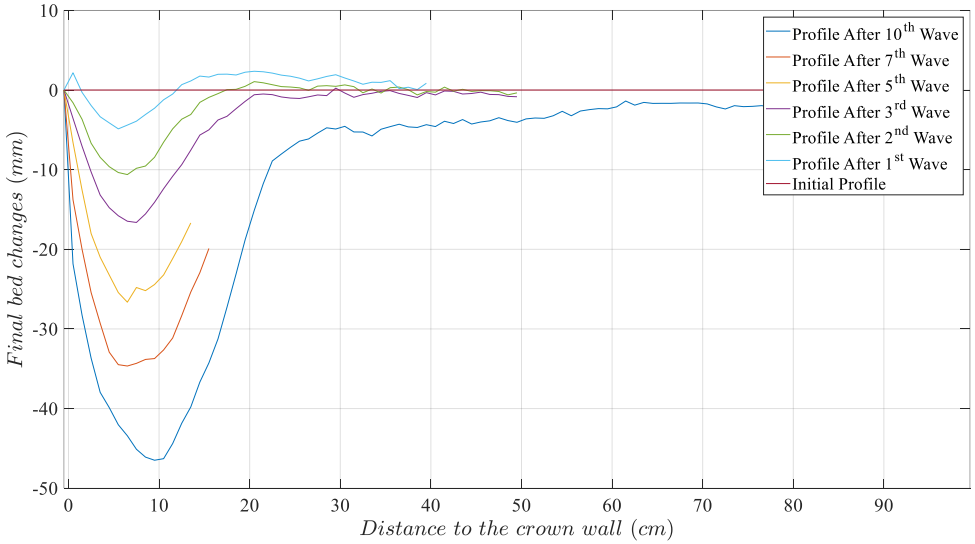

Figure 6.1 Scour Profile Evolution of Test 1

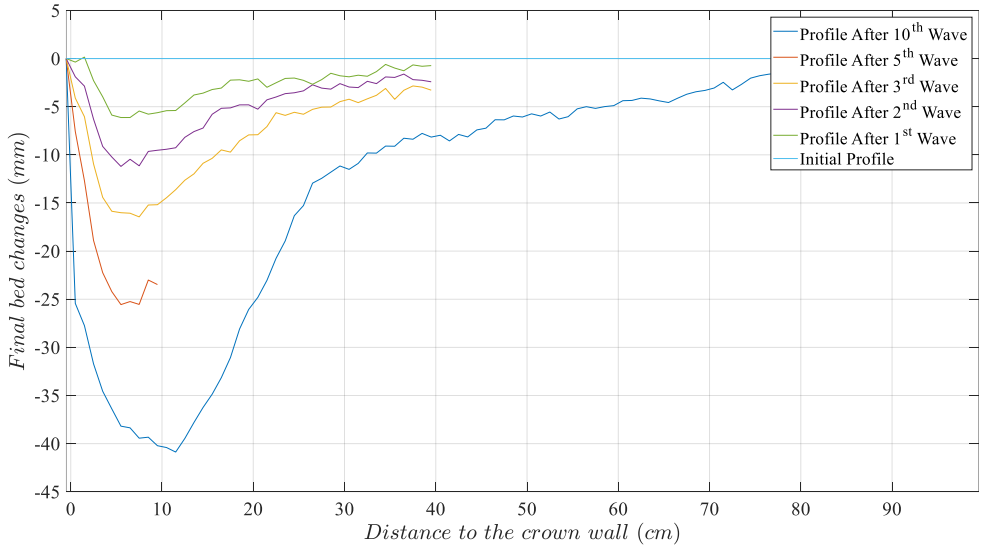

Figure 6.2 Scour Profile Evolution of Test 2

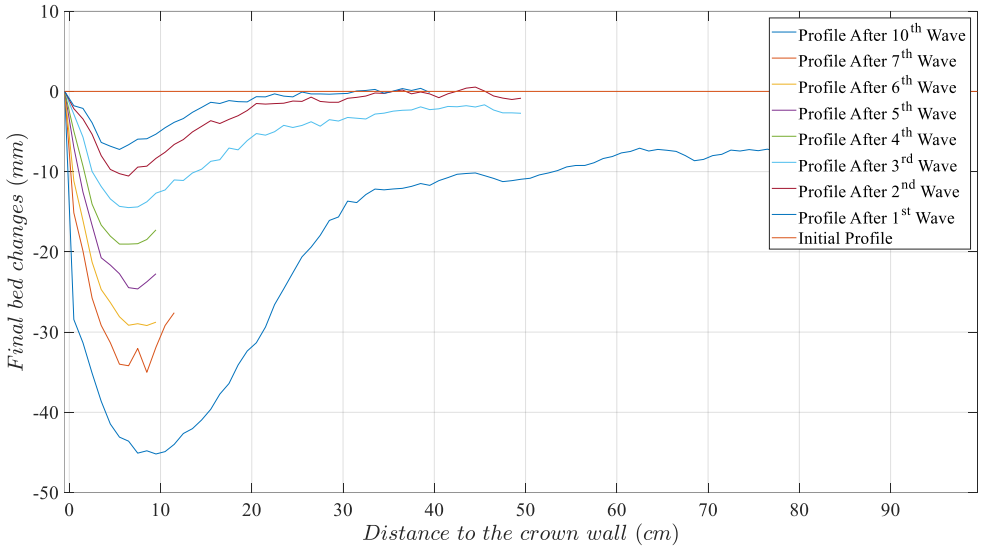

Figure 6.3 Scour Profile Evolution of Test 3

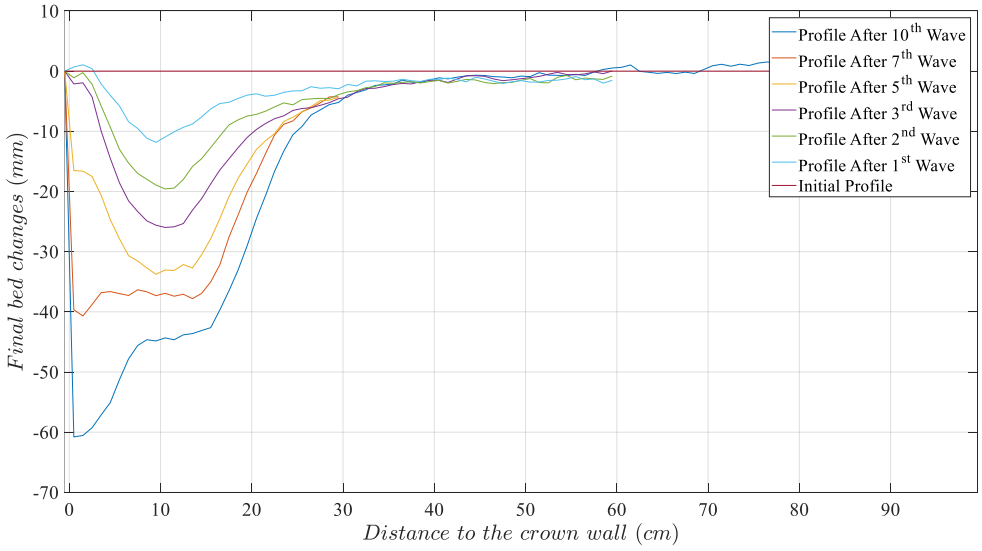

Figure 6.4 Scour Profile Evolution of Test 4

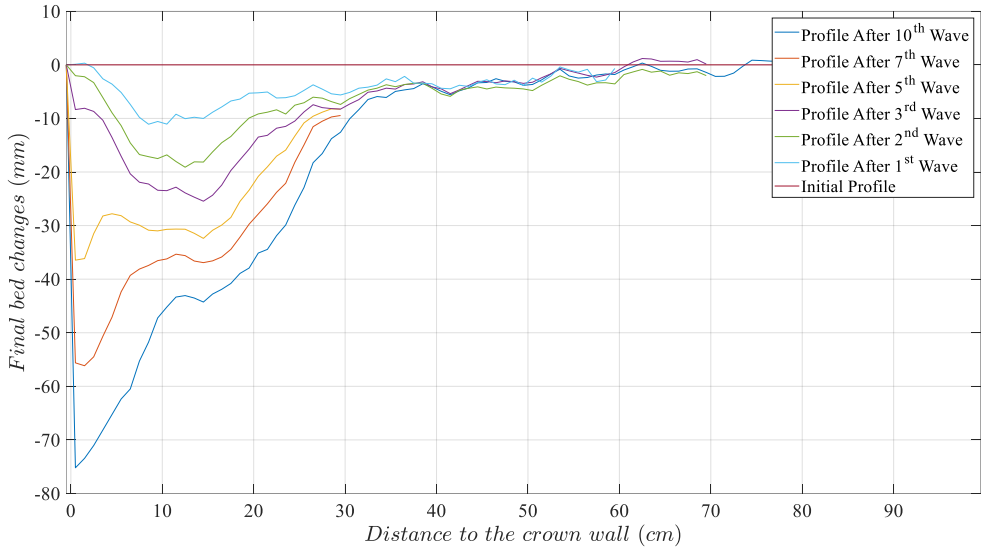

Figure 6.5 Scour Profile Evolution of Test 5

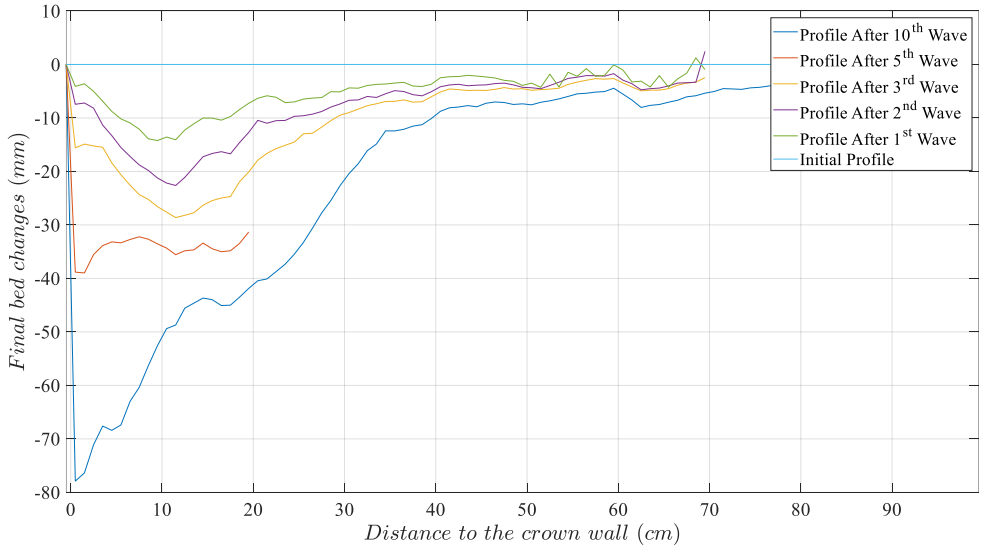

Figure 6.6 Scour Profile Evolution of Test 6

B. Rear Side Scour Formations for $d_{50} = 0.66\ mm$

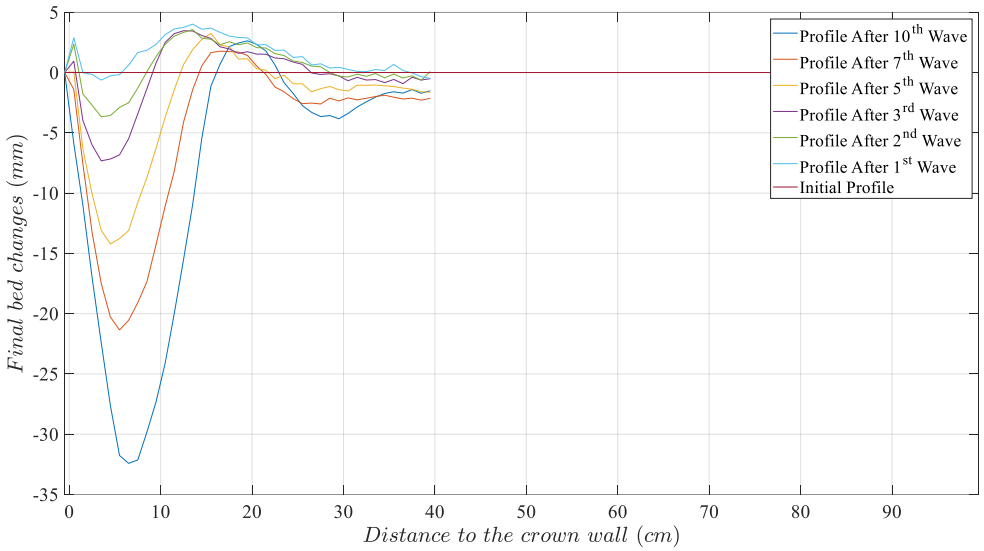

Figure 6.7 Scour Profile Evolution of Test 7

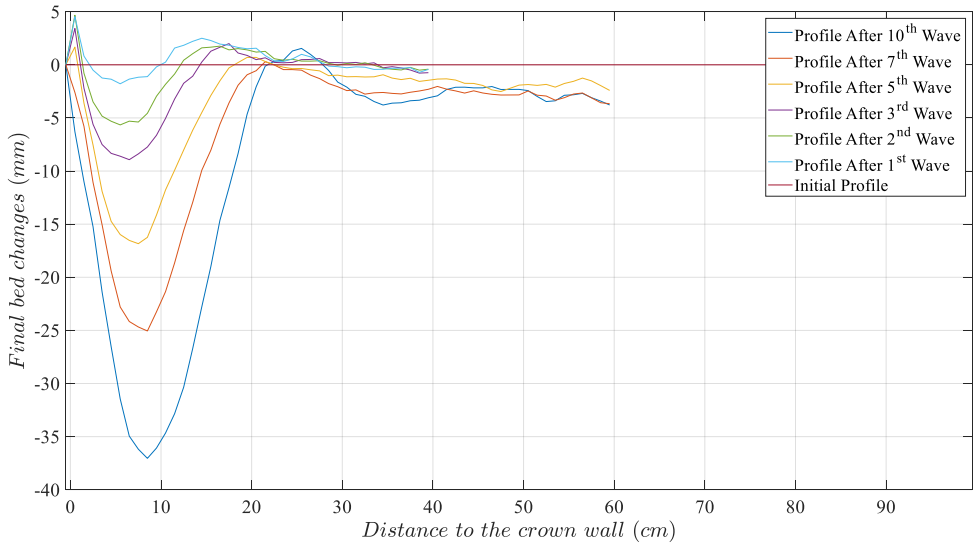

Figure 6.8 Scour Profile Evolution of Test 8

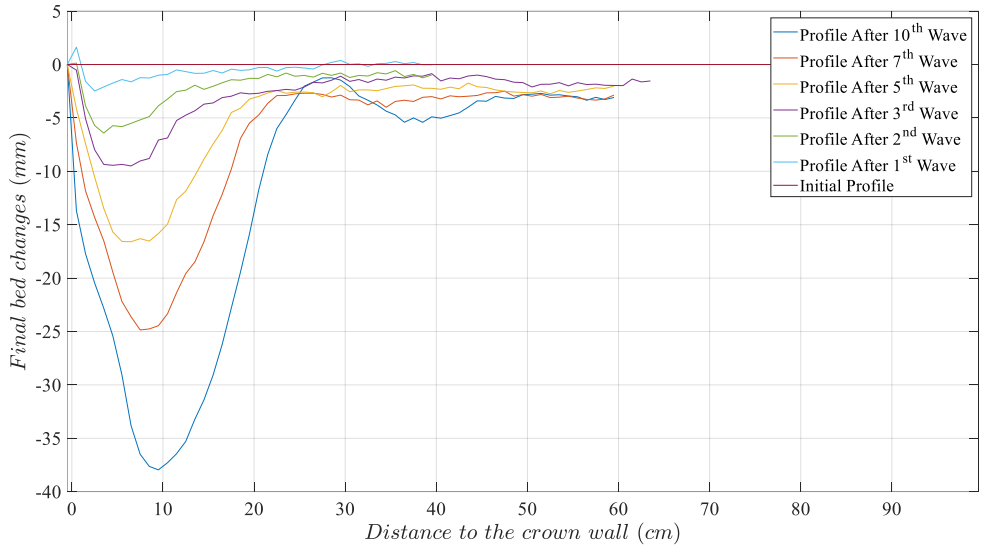

Figure 6.9 Scour Profile Evolution of Test 9

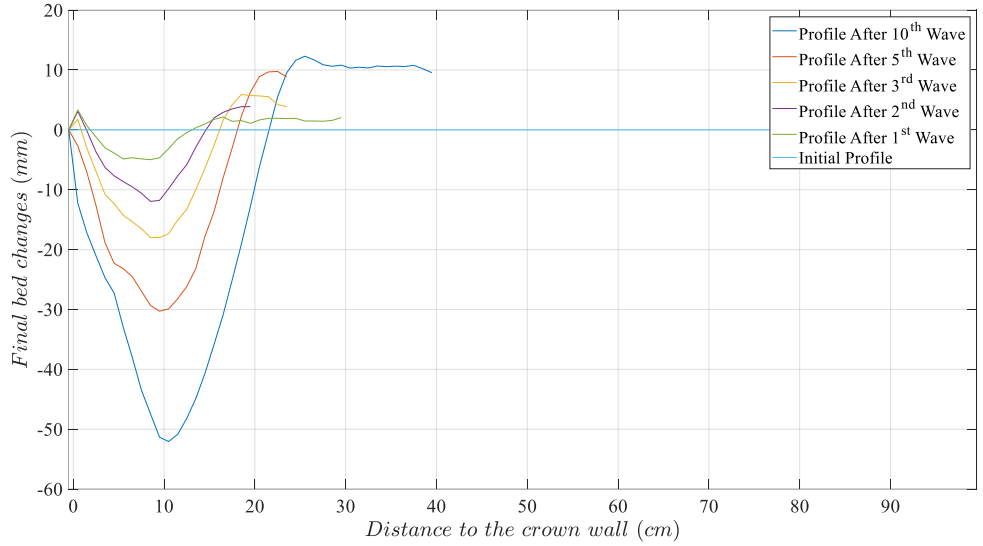

Figure 6.10 Scour Profile Evolution of Test 10

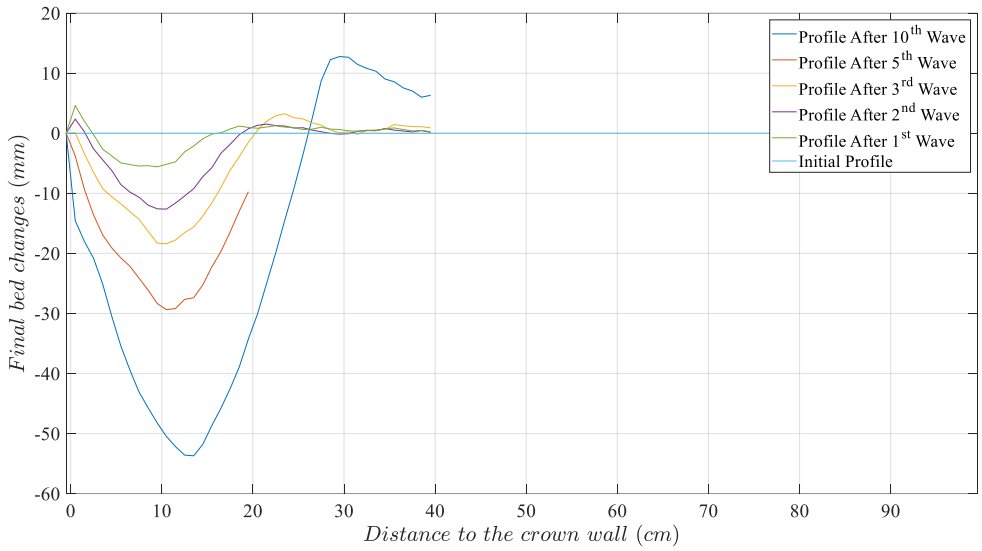

Figure 6.11 Scour Profile Evolution of Test 11

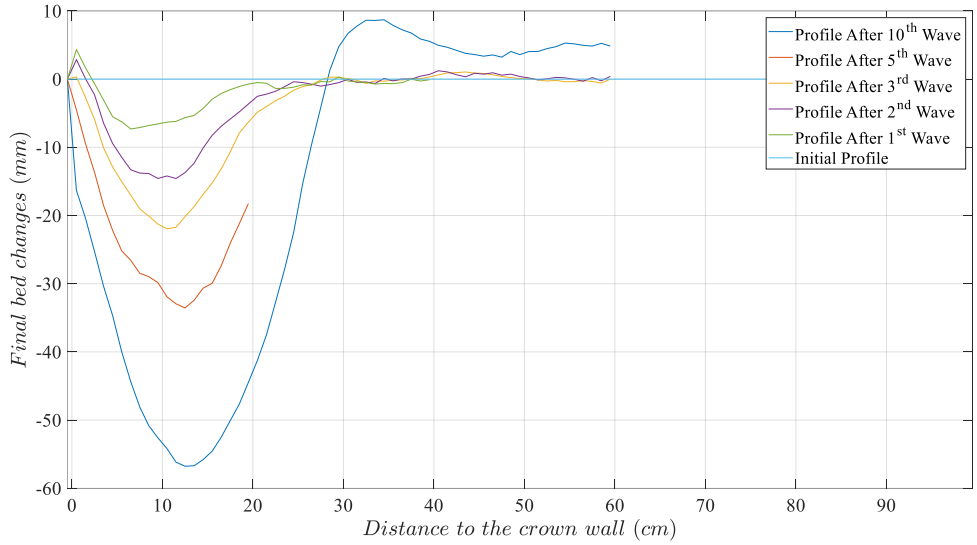

Figure 6.12 Scour Profile Evolution of Test 12

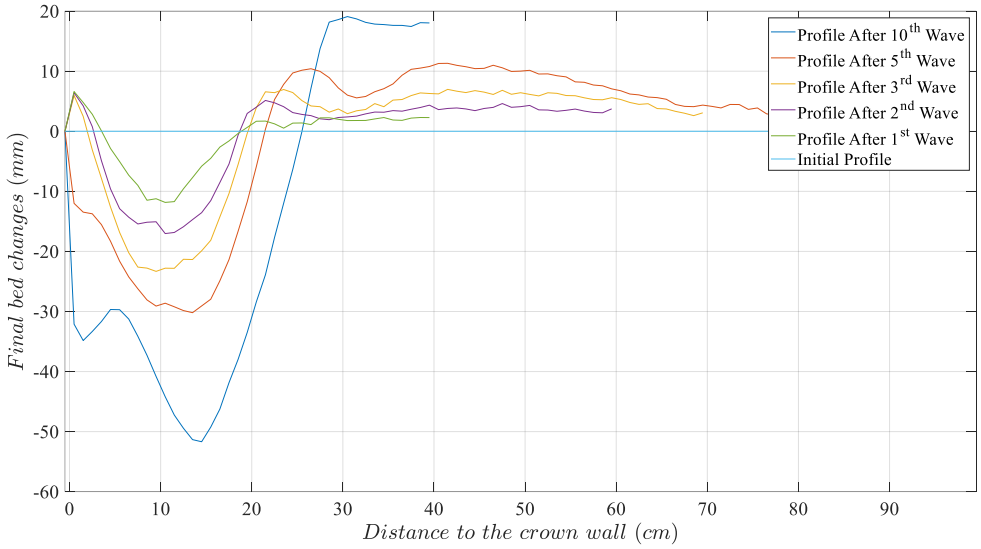

Figure 6.13 Scour Profile Evolution of Test 13

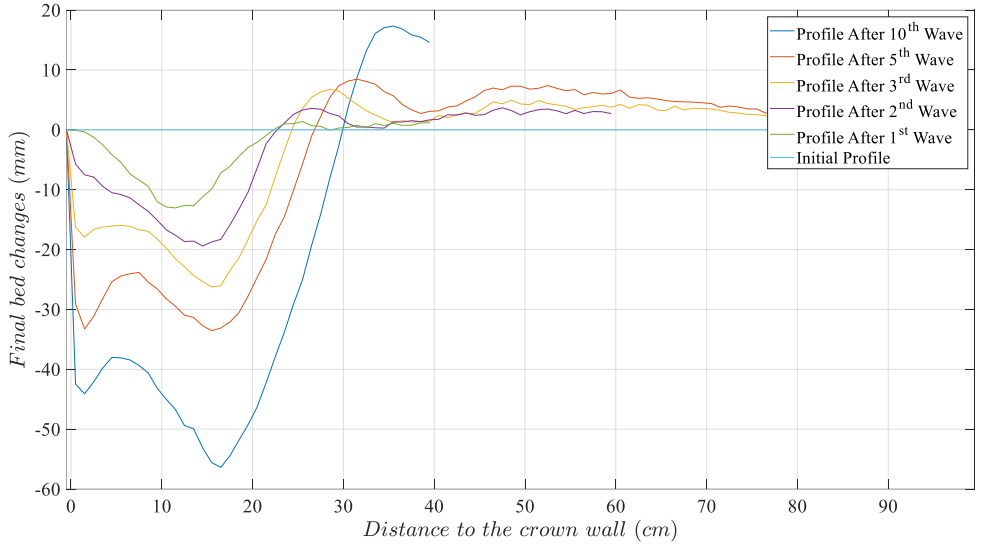

Figure 6.14 Scour Profile Evolution of Test 14

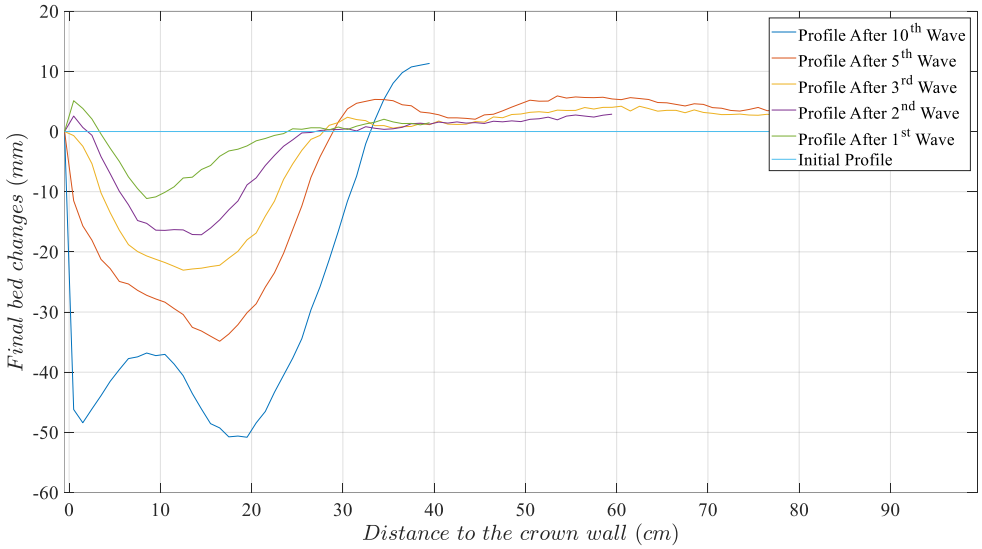

Figure 6.15 Scour Profile Evolution of Test 15

C. Rear Side Scour Formations for $d_{50} = 3.35\ mm$

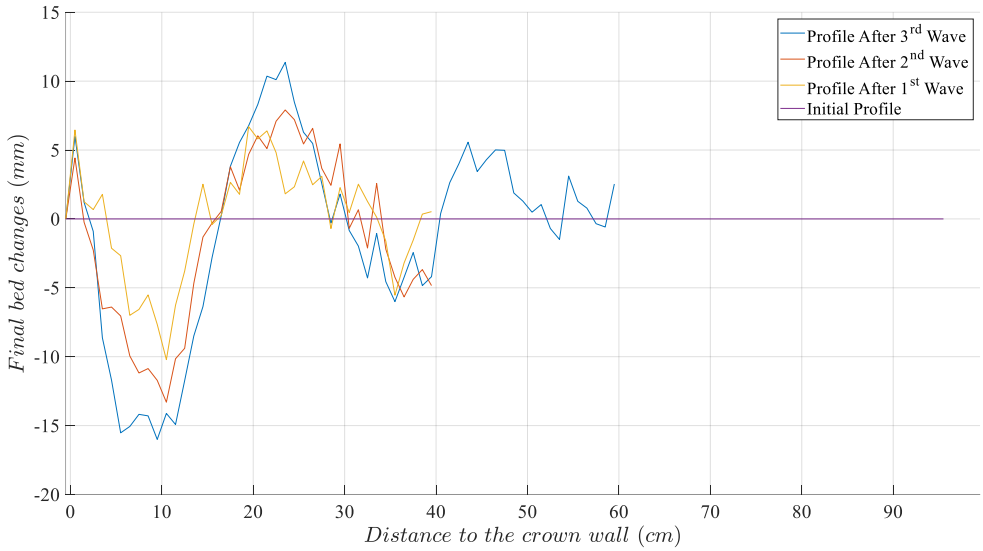

Figure 6.16 Scour Profile Evolution of Test 16

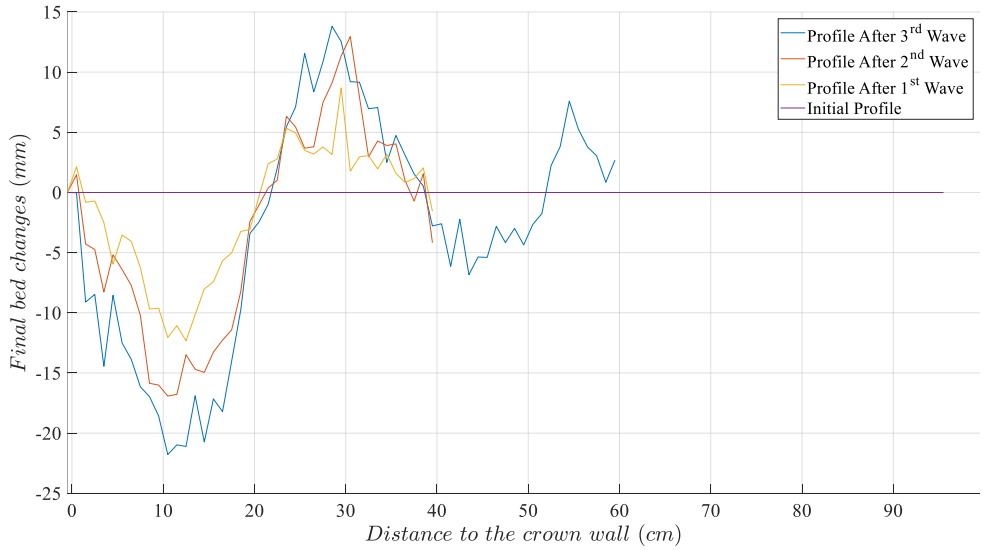

Figure 6.17 Scour Profile Evolution of Test 17

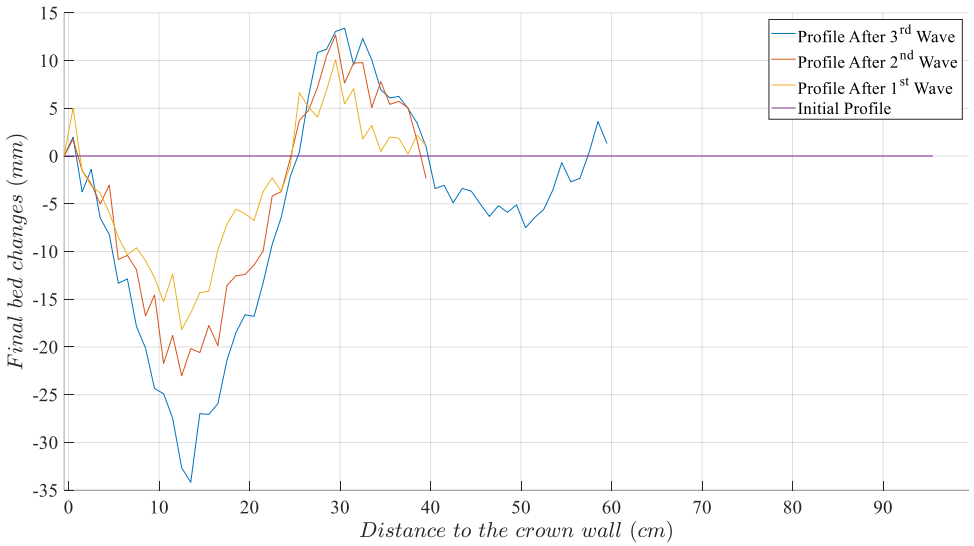

Figure 6.18 Scour Profile Evolution of Test 18